LAPPEENRANTA UNIVERSITY OF TECHNOLOGY
School of Technology
Mechanical Engineering

Jukka-Pekka Järvinen

WELDING OF ADDITIVELY MANUFACTURED STAINLESS STEEL PARTS: COMPARATIVE STUDY BETWEEN SHEET METAL AND SELECTIVE LASER MELTED PARTS

Examiners: Professor Antti Salminen
M.Sc. (Econ. & Bus. Adm.), M.Sc. (Tech.) Anne Kalliosaari

ABSTRACT

LAPPEENRANTA UNIVERSITY OF TECHNOLOGY
School of Technology
Mechanical Engineering

Jukka-Pekka Järvinen

WELDING OF ADDITIVELY MANUFACTURED STAINLESS STEEL PARTS: COMPARATIVE STUDY BETWEEN SHEET METAL AND SELECTIVE LASER MELTED PARTS

Master's Thesis

2014

68 pages, 44 figures, 13 tables, and 2 appendices

Examiners: Professor Antti Salminen
M.Sc. (Econ. & Bus. Adm.), M.Sc. (Tech.) Anne Kalliosaari

Keywords: Additive manufacturing, selective laser melting, welding, laser, stainless steel

Additive manufacturing is a fast growing manufacturing technology capable of producing complex objects without the need for conventional manufacturing process planning. During the process the work piece is built by adding material one layer at a time according to a digital 3D CAD model. At first additive manufacturing was mainly used to make prototypes but the development of the technology has made it possible to also make final products.

Welding is the most common joining method for metallic materials. As the maximum part size of additive manufacturing is often limited, it may sometimes be required to join two or more additively manufactured parts together. However there has been almost no research on the welding of additively manufactured parts so far, which means that there has been very little information available on the possible differences compared to the welding of sheet metal parts.

The aim of this study was to compare the weld joint properties of additively manufactured parts to those of sheet metal parts. The welding process that was used was TIG welding and the test material was 316L austenitic stainless steel. Weld joint properties were studied by making tensile, bend and hardness tests and by studying the weld microstructures with a microscope.

Results show that there are certain characteristics in the welds of additively manufactured parts. The building direction of the test pieces has some impact on the mechanical properties of the weld. Nevertheless all the welds exhibited higher yield strength than the sheet metal welds but at the same time elongation at break was lower. It was concluded that TIG welding is a feasible process for welding additively manufactured parts.

TIIVISTELMÄ

Lappeenrannan teknillinen yliopisto
Teknillinen tiedekunta
Konetekniikka

Jukka-Pekka Järvinen

LISÄÄVÄLLÄ VALMISTUKSELLA RUOSTUMATTOMASTA TERÄKSESTÄ TEHTYJEN KAPPALEIDEN HITSAUS: VERTAILEVA TUTKIMUS VALSSATTUJEN LEVYJEN JA LASERSULATUKSELLA VALMISTETTUJEN KAPPALEIDEN HITSAUKSESTA

Diplomityö

2014

68 sivua, 44 kuvaa, 13 taulukkoa ja 2 liitettä

Tarkastajat: Professori Antti Salminen
KTM, DI Anne Kalliosaari

Hakusanat: Lisäävä valmistus, 3D-tulostus, hitsaus, laser, ruostumaton teräs

Lisäävä valmistus on nopeasti kasvava valmistusmenetelmä, jolla voidaan tehdä monimutkaisia kappaleita ilman tarvetta perinteiselle valmistusprosessien suunnittelulle. Prosessin aikana kappale valmistetaan lisäämällä materiaalia kerroksittain digitaalisen 3D CAD-mallin mukaan. Alun perin lisäävää valmistusta käytettiin lähinnä prototyyppien tekemiseen, mutta menetelmän kehittymisen myötä sitä on alettu käyttämään myös lopputuotteiden valmistamiseen.

Hitsaus on metallisten materiaalien yleisin liittämismenetelmä. Valmistettavien kappaleiden koko on usein varsin rajallinen lisäävässä valmistuksessa, joten kappaleita voidaan joutua liittämään toisiinsa. Lisäävällä valmistuksella tehtyjen kappaleiden hitsausta ei kuitenkaan ole toistaiseksi juuri tutkittu, joten hitsauksen mahdollisista eroavaisuuksista tavallisen levymateriaalin hitsaukseen verrattuna ei ole ollut tietoa.

Työn tavoitteena oli vertailla lisäävällä valmistuksella tehtyjen kappaleiden hitsausliitosten ominaisuuksia samankaltaisen levymateriaalin hitsausliitoksiin. Hitsausprosessina käytettiin TIG-hitsausta ja koemateriaalina 316L austeniittista ruostumatonta terästä. Hitsausliitosten ominaisuuksia tutkittiin veto-, taivutus- ja kovuuskokeiden avulla sekä tarkastelemalla hitsien mikrorakenteita mikroskoopilla.

Tulokset osoittavat lisäävällä valmistuksella tehtyjen kappaleiden hitseissä tiettyjä ominaispiirteitä. Koekappaleiden valmistussuunta vaikuttaa jonkin verran liitoksen mekaanisiin ominaisuuksiin. Liitosten myötöluujudet olivat korkeampia kuin levymateriaalin hitsausliitoksissa, mutta samanaikaisesti murtovenymät olivat matalampia. Yhteenvetona todettiin, että lisäävällä valmistuksella tehtyjen kappaleiden liittäminen toisiinsa on mahdollista TIG-hitsausta käyttäen.

ACKNOWLEDGEMENTS

This Master's thesis was carried out at Lappeenranta University of Technology Laboratory of Laser Processing as a part of the Finnish Metals and Engineering Competence Cluster (FIMECC)'s program MANU - Future digital manufacturing technologies and systems.

First I want to thank Professor Antti Salminen not only for all the advice and guidance during the writing process but also for providing me with this interesting topic, which proved to be quite challenging at times. I would like to thank the supervisor of the thesis Anne Kalliosaari for always being helpful and ready to give suggestions and comments. Your efforts really helped push this project onward. The rest of the staff at LUT Laser also deserve my gratitude for offering me a friendly working environment and for all the help and good times I had when I worked there.

I would like to say a big thank you to all the personnel at LUT Welding Laboratory who contributed to this study, especially Antti Kähkönen for all the help with the welding experiments and Antti Heikkinen for helping me with the micrographic examination of the test pieces. Your practical knowledge and experience was of great help during the experimental part of the study.

A special mention goes to all the friends I have studied and spent time with during my university studies for making this time truly memorable. Lastly I want to take this opportunity to thank my parents Eija and Paavo and my brother Kimmo for all the support during these years. You have given me invaluable advice and help to get through difficult times and to make this possible.

Lappeenranta, 3rd of December 2014

Jukka-Pekka Järvinen

TABLE OF CONTENTS

LIST OF SYMBOLS AND ABBREVIATIONS

µm	Micrometer
3D	Three Dimensional
A	Ampere
AC	Alternating Current
AM	Additive Manufacturing
Ar	Argon
ASTM	American Society for Testing and Materials
C	Carbon
CAD	Computer Aided Design
$(COOH)_2$	Oxalic Acid
Cr	Chromium
Cr_{eq}	Chromium Equivalent
Cu	Copper
DCEN	Direct Current Electrode Negative
DCEP	Direct Current Electrode Positive
DMLS	Direct Metal Laser Sintering
FBB	Face Bend Test Specimen for Butt Weld
GPa	Gigapascal
GTAW	Gas Tungsten Arc Welding
H	Hydrogen
HAZ	Heat Affected Zone
He	Helium
HRB	Hardness Rockwell B
HV	Hardness Vickers
kJ	Kilojoule
kp	Kilopond
l	Liter
min	Minute
mm	Millimeter
Mn	Manganese

Mo	Molybdenum
MPa	Megapascal
N	Nitrogen
Nb	Niobium
Ni	Nickel
Ni_{eq}	Nickel Equivalent
nm	Nanometer
P	Phosphorus
P	Power
PBF	Powder Bed Fusion
RBB	Root Bend Test Specimen for Butt Weld
RP	Rapid Prototyping
s	Second
S	Sulfur
Si	Silicon
SLM	Selective Laser Melting
SLS	Selective Laser Sintering
STL	Standard Tessellation Language
TIG	Tungsten Inert Gas
U	Scan Speed
V	Volt
W	Watt
WPS	Welding Procedure Specification

1 INTRODUCTION

1.1 Background

Additive manufacturing, also known as 3D printing, has gained a lot of worldwide attention over the past few years. Both the recent improvements in 3D printing machinery and new process innovations have made the technology more appealing not only to industrial manufacturers but normal households as well. Even though most of the hype concerning 3D printing has only been around for a few years, the basic concept of additive manufacturing was already invented in the 1980s.

At first additive manufacturing was mainly used in the making of prototypes and models, hence it was called Rapid Prototyping (RP). As its name suggests, the purpose of rapid prototyping is to quickly create a prototype and this way allow different ideas to be tested during the development process. However, as additive manufacturing technology improved, so did the quality of manufactured parts and it became possible to make final products as well.

The additive manufacturing of metallic materials offers many possibilities for industrial use. Weight optimization and the making of complex geometries are some of the advantages of the technology. Due to the nature of the process however, the dimensions of the manufactured objects are often quite limited. Occasionally joining two additively manufactured parts together may be required or a part needs to be joined with an existing structure. This brings up the topic of welding, which is the most common joining method for metallic materials. Welding itself has been studied extensively for decades but research on the welding of additively manufactured components has been very scarce.

1.2 Objectives and limitations

The main objective of this thesis is to gain knowledge about the welding of additively manufactured stainless steel components and whether the properties of the weld joints differ from those of conventional cold rolled stainless steel of similar composition. The properties of additively manufactured parts depend on the building direction so one objective is to study if the building direction also affects the properties of weld joints. So

far there have been very few publications on this topic and so this thesis will be among the very first. Also any other possible differences concerning for example welding process parameters will be studied.

Being that this is a large subject and will require lots of studying to fully understand all the different aspects of it, this thesis will have to focus on certain things. The test material is stainless steel 316L which is a common material in many industrial applications and often used in welding. The properties of welds between two additively manufactured parts will be compared to the properties of welds between two sheet metal test pieces. Weld joints between rolled and AM test pieces are left out of this study. The welding process that was used was Tungsten Inert Gas (TIG) welding, which is a common process for welding thin sections of stainless steel. TIG welding is also a versatile process capable of producing very high quality welds.

1.3 Research methods

The thesis is divided into two main parts: theoretical and experimental part. In the theoretical part the basic concept of additive manufacturing, TIG welding and cold rolling of stainless steel sheets, as well as the properties and welding characteristics of austenitic stainless steels, are introduced. Finally the principles of destructive tests such as tensile, bend and hardness test are explained. The theoretical part is based mainly on scientific research articles and also on textbooks.

In the experimental part, test pieces were made out of stainless steel powder with Selective Laser Melting (SLM) and then welded together. After this a series of destructive tests was executed, including tensile, bend and hardness tests, in order to examine the mechanical properties of the weld joints. The same tests were also done to sheet metal pieces of similar stainless steel material. Finally, the weld joints were examined with a microscope to gain knowledge about the microstructural changes that take place during welding.

2 ADDITIVE MANUFACTURING PROCESS

Additive manufacturing technology in short is a manufacturing process in which material is added in layers to form a work piece. This kind of approach practically eliminates the need for manufacturing process planning which usually takes more time the more complex the manufactured object is. With additive manufacturing it is generally much easier to produce complex objects as opposed to conventional manufacturing methods which rely on material removal. (Gibson et al. 2010, p. 1-2.)

2.1 Process chain

The work piece is built using a digital 3D CAD model which represents the external surface geometry of the part. The model is usually made with CAD modeling software but a process called 3D scanning can also be used. With 3D scanning it is possible to analyze and collect data on the shape of an object by using a scanner device. The data can then be used to create a point cloud and further a solid CAD model of the scanned object. Next the model is converted into STL file format which is the standard format in most AM machines. After this the model is sliced into thin layers, each layer representing a cross-section of the part. The part is built one layer at a time according to the sliced CAD model. However as the part is built layer by layer, the result will be an approximation of the 3D model and not an identical copy of it. As such, by using thinner layers the resulting part will resemble the original model more closely. In the actual build process a layer of material is deposited and then selectively consolidated by using a scanning laser beam. Once the building is complete the part is removed from the machine. At this point there may be a need for additional post processing such as support structure removal, heat treatment or surface finishing. (Gibson et al. 2010, p. 4-5, Gu et al. 2012, p. 133.) The different phases of additive manufacturing process in general are presented in Figure 1.

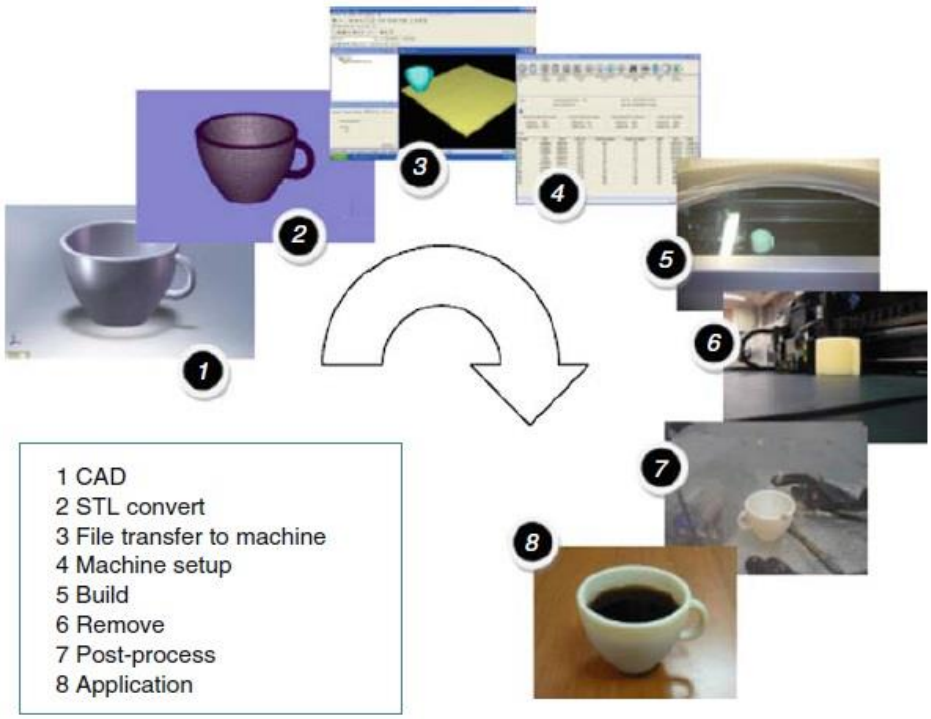

Figure 1. The different phases of the additive manufacturing process (Gibson et al. 2010, p. 4).

2.2 Powder bed fusion process

Powder bed fusion (PBF) is a type of additive manufacturing process in which a layer of powder is spread into a build area and then a fusion between the powder particles is selectively caused by using a thermal source. The region where the powder fusion is caused in each layer is controlled according to the CAD model. The adding and smoothing of additional powder layers needs to be done carefully as the even distribution of powder contributes to the success of the final product. PBF is a flexible process when it comes to manufacturing materials, as the range of materials includes for example metals, polymers, ceramics and composites. Also due to good material properties, powder bed fusion is more and more used to directly make final products without the need for post-processing. However metallic materials often require support structures because of the residual stresses that are formed during the process. Support structures offer mechanical support for overhang features and conduct excessive heat away from the part, thus preventing it from warping. (Gibson et al. 2010, p. 103, 140.)

The powder bed fusion process is further divided into several processes which all share the same basic principle. The major difference between laser sintering and laser melting processes is in the material melting mechanism. In laser sintering processes the powder is melted only partially whereas in laser melting the powder is completely melted. Nevertheless, different institutions and companies use different names for additive manufacturing processes, such as Direct metal laser sintering (DMLS), Selective laser sintering (SLS) and Selective laser melting (SLM). (Gu et al. 2012, p. 134-135.) Despite their names, in all of the aforementioned processes the powder material is completely melted. The amount of names for metallic powder bed based processes can be confusing, but the term selective laser melting will be used in this study to describe the process. Figure 2 presents a schematic view of the SLM system, which can be applied to all powder bed fusion processes in general.

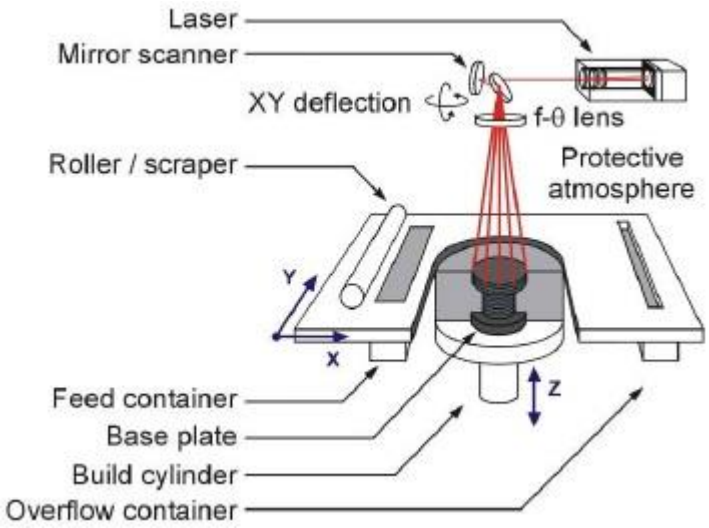

Figure 2. A schematic of the SLM system (Kruth et al. 2010, p. 1).

2.3 Microstructure of parts made with selective laser melting

Powder material forms the base for selective laser melting. Even though the actual manufacturing process defines the final properties of the component, the quality of the powder also affects the outcome. The main features of the powder material, such as chemical composition, particle size and shape and particle size distribution, are controlled by the powder manufacturing process. Powders manufactured with gas atomization have a spherical particle shape, which is usually desirable as it allows the powder to be spread in a

way that dense parts can be made. Therefore gas atomization is usually the preferred powder production process. (Klar & Samal 2007, p. 23-24.) A microscopic view of gas atomized 316L austenitic stainless steel powder particles can be seen in Figure 3.

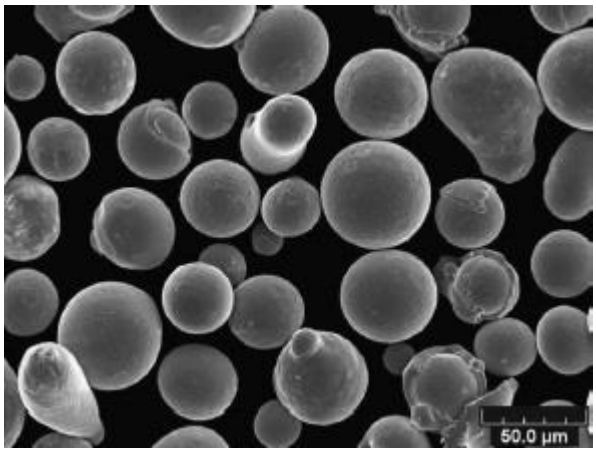

Figure 3. 316L stainless steel powder particles with a 300x magnification (Zhang et al. 2013, p. 22).

Due to the nature of the SLM process where metal powder is melted into a small melt pool that solidifies quickly, the microstructure of the finished component may contain some unique features such as non-equilibrium phases. By taking advantage of these microstructural features it may be possible to optimize the properties of the material more effectively. (Kruth et al. 2010, p. 1-2, Murr et al. 2012, p. 2.)

The mechanical properties of additively manufactured objects depend mainly on the solidification microstructure. In laser based additive manufacturing processes the heating and cooling of the material is very rapid and takes place in a small area. During the process the conduction of heat causes a fast rate of quenching which in turn leaves little time for grain growth. Also the melt pool geometry, which is affected by heat transfer and fluid flow, influences the final microstructure of the part. (Gu et al. 2012, p. 155, Kruth et al. 2010, p. 1.) Figure 4 presents a schematic view of the SLM process.

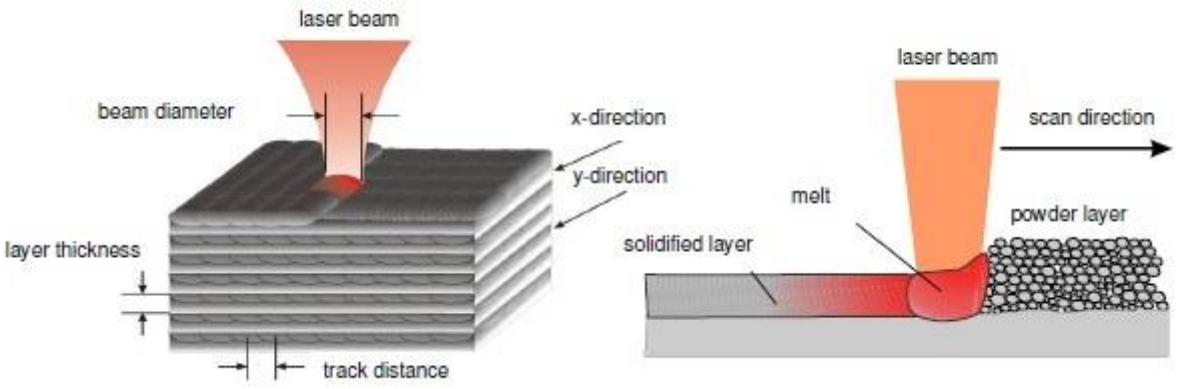

Figure 4. A schematic view of the SLM process (Meiners 2011, p. 10).

An important feature in the microstructure of additively manufactured objects is that the microstructure is different between the bottom and the top of the part. This is mainly due to the fact that at the bottom of the part heat conduction and cooling is higher than at the top of the part. Heat accumulates into the top of the part and this causes variation in the microstructures along the height direction. At the bottom of the part where conductive cooling is highest, the average grain size is smaller than at the top of the part. (Gu et al. 2012, p. 156.)

Kruth et al. (Kruth et al. 2010, p. 4-6.) compared some of the mechanical properties of parts made with SLM to those of bulk materials manufactured with conventional processes. It was concluded that generally the properties were comparable apart from a few exceptions. The main difference is that the toughness values of SLM parts are lower than those of bulk materials and especially in the case of 316L stainless steel the toughness values were considerably inferior. The reason for this was attributed to defects, pores, impurities and brittle microstructural phases in the SLM parts.

The density of the parts depends on the parameters that are used during manufacturing. Recent studies show that near full density (>99 %) parts can be made by optimizing the process parameters. Kamath et al. (Kamath et al. 2014, p. 74-76) studied the porosity of 316L stainless steel parts and were able to manufacture parts with a relative density of around 99.8 %, although there was a little error in the measurement of the density. In

Figure 5 a microscopic view of the polished and etched surface of an SLM part can be seen.

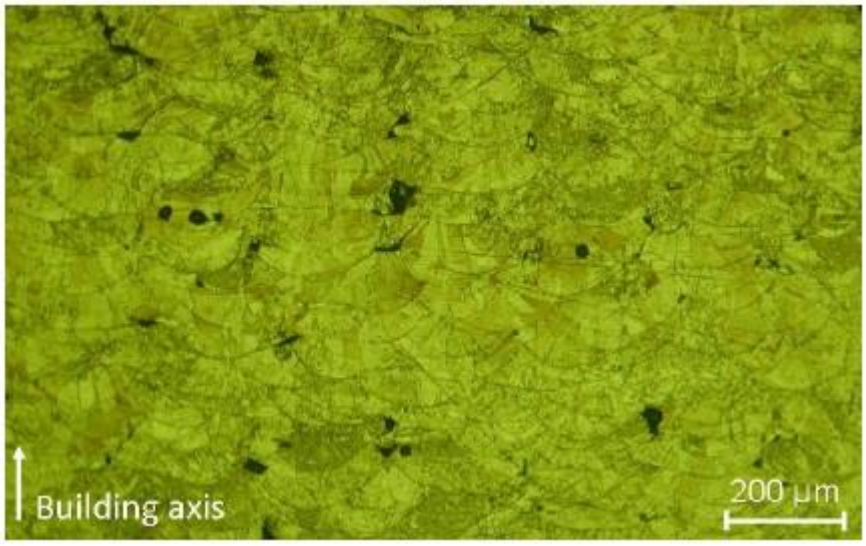

Figure 5. Frontal microscopic view of an SLM part made out of 316L stainless steel. The surface has been polished and etched. (Kruth et al. 2010, p. 7.)

It can be seen in Figure 5 that due to the laser scan tracks overlapping, each molten track is connected to the other surrounding tracks. The powder particles are entirely fused together although there is a little porosity which can be seen as black dots. Based on Figure 5 it can also be noticed that the depth of the melt pool has been around 100 µm, which is considerably higher than the 30 µm layer thickness that was used. (Kruth et al. 2010, p. 7.)

In powder bed based processes the microstructure in the exterior surface of a processed part is generally different compared to the inner microstructure due to a phenomenon called balling effect. During the process laser energy forms a continuous liquid scan track by melting powder particles but surface tension forces in the molten metal pool may cause balling of the material along the scan track, as seen in Figure 6. (Gibson et al. 2010, p. 136, Gu et al. 2012, p. 154.)

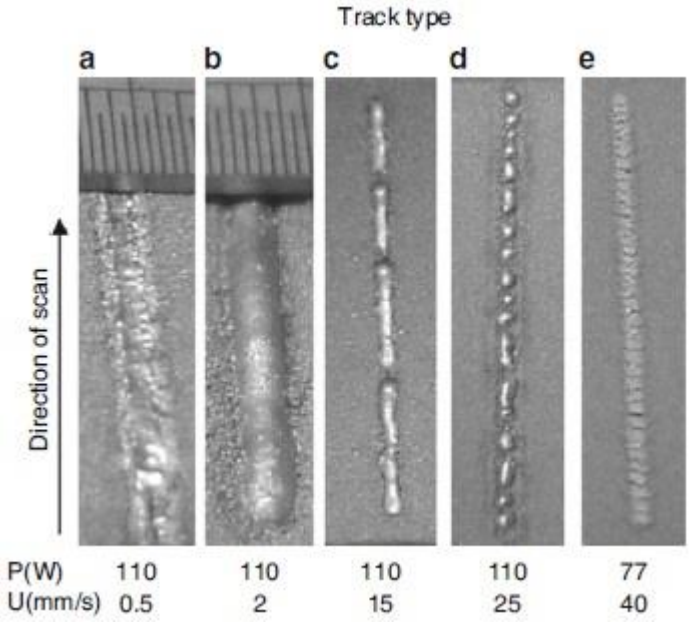

Figure 6. Test tracks at different power and scan speed combinations. Balling of the material can be seen in track type D. (Gibson et al. 2010, p. 137.)

As it can be seen from Figure 6 the scan tracks become more and more broken as the scanning speed increases. Balling effect can cause poor bonding of layers, non-uniform deposition of new powder layers and even delamination, which means that the consolidated layers get separated. Balling effect can be prevented by reducing scan speed and increasing power. (Gu & Shen 2009, p. 2903, Gu et al. 2012, p. 154-155.)

3 COLD ROLLING OF STAINLESS STEEL SHEETS

In steel manufacturing the molten metal is first cast into large slabs and then hot rolled between one or more rolls in a high temperature. This reduces the thickness of the slab and increases its length. After cooling the steel sheet can already be used as such, but it is usually desirable to improve the mechanical properties and surface quality of the material by cold rolling it. Cold rolling is a metal forming process that is used to achieve good surface quality and narrow dimensional tolerances in sheet metal products. It also makes the steel stronger by increasing its yield strength and hardness but at the same time it becomes more brittle. Because of this the steel needs to be annealed which restores the ductility of the material that was lost during the cold rolling process. During the annealing phase recrystallization takes place in the distorted microstructure which causes new grains to grow in place of the elongated grains. (Colás et al. 2004, p. 56-58.) Figure 7 shows the hot rolling, cold rolling and annealing process chain.

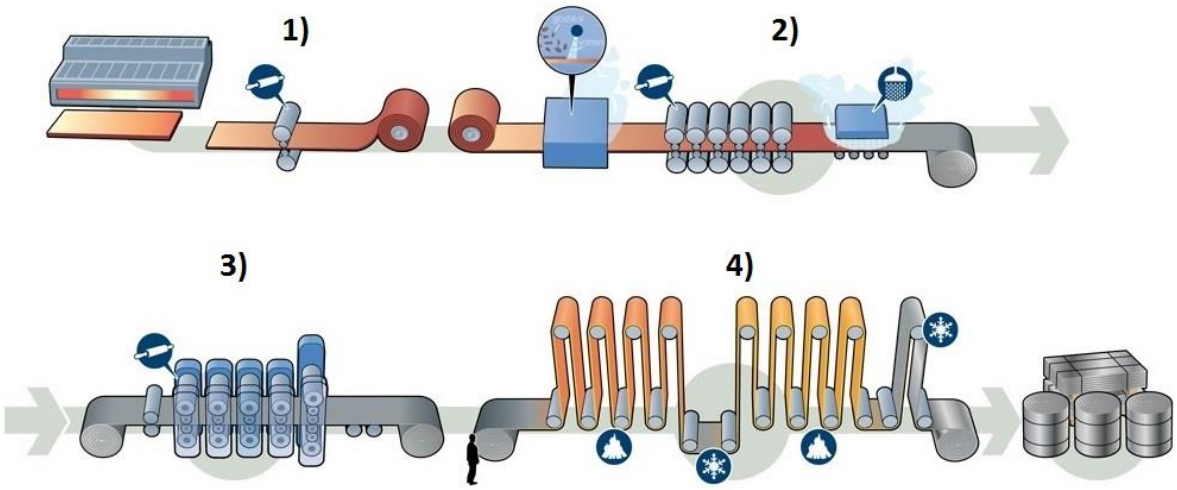

Figure 7. The main phases of sheet steel forming process: 1) the thickness of the slab is substantially reduced in the roughing mill; 2) hot rolling and cooling of the sheet; 3) cold rolling; 4) annealing, quenching and tempering of the sheet (Modified from SSAB 2011).

During cold rolling the grains in the microstructure of the steel elongate along the rolling direction. However, the grains do not grow in size since recrystallization does not occur in

a low temperature. This results in an anisotropic, directional microstructure which has different mechanical properties in different directions, as seen in Figure 8. (Colás et al. 2004, p. 57.) Before the cold rolling phase the microstructure of 316L stainless steel is fully austenitic but during the rolling process some of the austenite starts to transform into strain-induced martensite as a result of work hardening. Martensite has very high strength and hardness, but it is also brittle which means that the ductility of the material needs to be restored after the cold rolling process. (Hedayati et al. 2010, p. 1019-1021.)

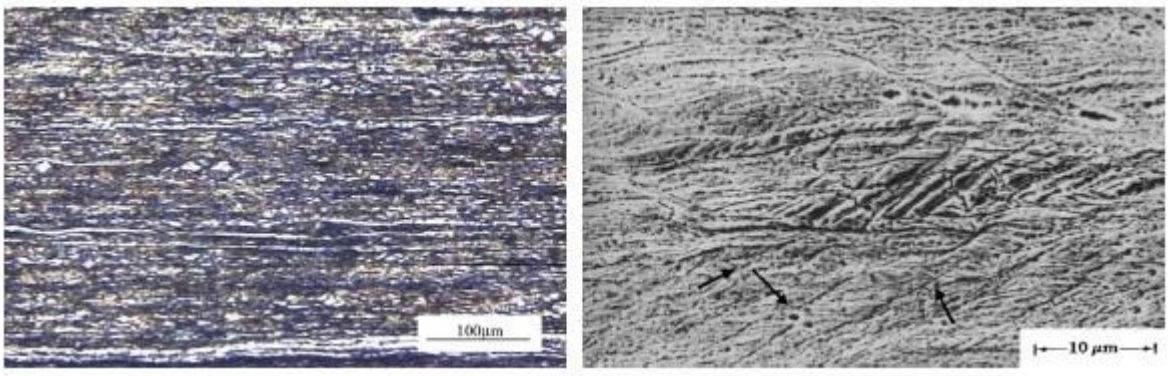

Figure 8. Micrographs of a 90 % cold rolled 316L stainless steel sheet showing a typical directional microstructure caused by the cold rolling process (Chowdhury et al. 2005, p. 3953).

Unlike most other types of steels, the properties of austenitic stainless steels are difficult to modify through thermo-mechanical processing because their microstructure consists of a single austenite phase. Traditional thermo-mechanical processes depend mainly on the phase transformation characteristics of the metal when it is heated and cooled down, but in austenitic stainless steels the austenite phase remains stable up to the liquidus temperature and no phase transformation occurs. The microstructure can be refined however with recrystallization annealing treatment. The cold rolled microstructure stores a large amount of energy which acts as the driving force for recrystallization. During annealing the material is heated to a temperature of around 900 °C which offers additional energy to the process and makes grain growth possible. (Kumar & Sharma 2013, p. 157-159.) Figure 9 presents partial recrystallization after annealing where deformed and elongated grains are transforming into finer grains.

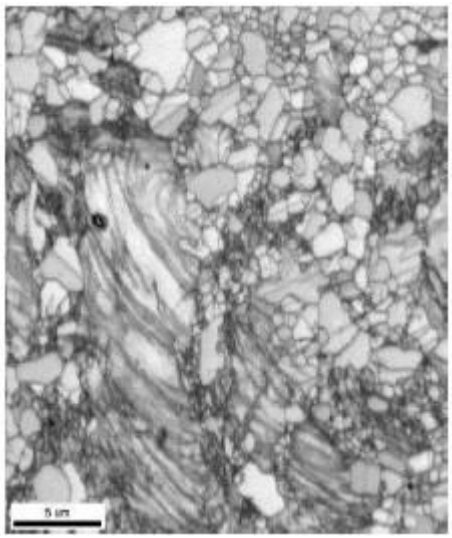

Figure 9. Partial recrystallization in the austenitic microstructure of cold rolled 316L stainless steel after 45 s annealing time at the temperature of 925 °C (Kumar & Sharma 2013, p. 159).

After annealing the microstructure consists of fine grained austenite which makes the material more ductile again and also some regions of residual cold deformed grains. The amount of residual deformed grains can be decreased with additional annealing cycles. (Kumar & Sharma 2013, p. 159-160.)

4 BASICS OF TUNGSTEN INERT GAS WELDING

Tungsten inert gas (TIG) welding, also known as Gas Tungsten Arc Welding (GTAW), is an arc welding process in which a nonconsumable tungsten electrode is used to generate the weld. The welding torch which holds the tungsten electrode is connected into a shielding gas supply and also to the welding machine which is the power source. The electrode inside the torch is cooled with water to prevent overheating. An inert shielding gas such as helium or argon is fed through a nozzle into the weld pool to protect it from the surrounding air. TIG welding can be autogenous but a filler metal may also be used for example when joining thicker materials. (Kou 2003, p. 13-14.) Figure 10 presents the process schematic and welding area of TIG welding.

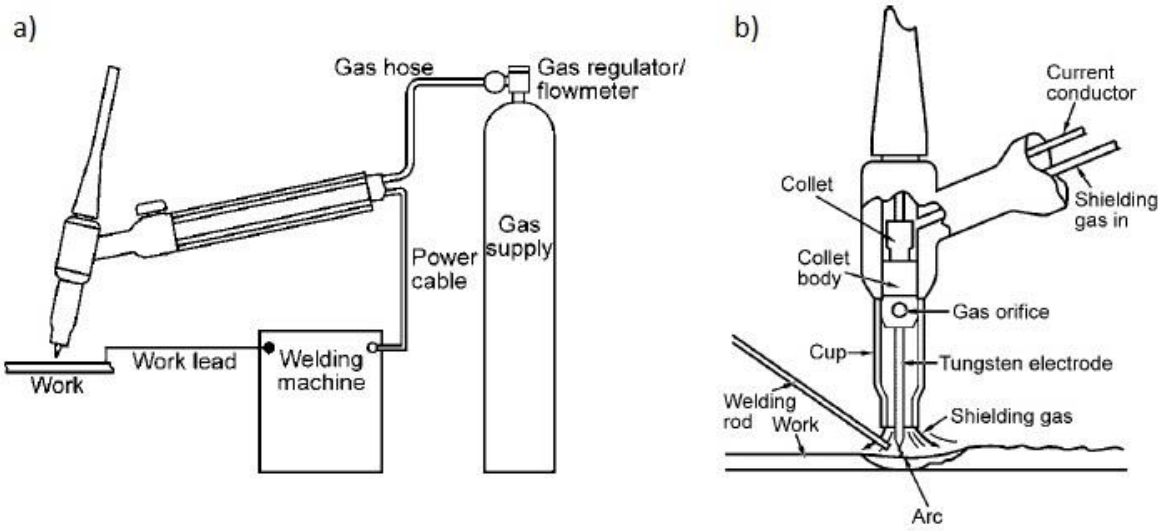

Figure 10. TIG welding: a) overall process schematic; b) enlarged welding area (Lienert et al. 2011, p. 344).

During the process an electric arc is created between the tungsten electrode and the work piece. In many other welding processes the filler metal also acts as the electrode and is therefore consumed during welding. However in TIG welding the electrode does not melt or transfer into the weld. As the arc current is primarily carried by electrons, the electrode tip emits electrons during welding which causes significant cooling in the tip. This cooling effect accompanied with the high melting point of tungsten (3410 °C) makes it possible for

the electrode to remain unmelted throughout the process. (Lienert et al. 2011, p. 349-350, Salkin et al. 2004, p. 113.)

Shielding gas is used to protect the molten weld pool and the welding electrode from the surrounding atmosphere. Argon is the most commonly used shielding gas for TIG welding since it is the least expensive option and it also offers excellent protection due to the fact that it is heavier than air, displacing the air around the weld. Helium as a shielding gas offers greater heating power than argon which can be beneficial when welding metals that have a high thermal conductivity. Sometimes a mixture of argon and helium is used to get a balance between the features of the two gases. (Lienert et al. 2011, p. 350, Salkin et al. 2004, p. 123-125.)

The TIG welding process can be operated in one of three modes: direct current with electrode negative (DCEN), direct current with electrode positive (DCEP) and alternating current (AC). The choice depends on the type and thickness of the material to be welded and each current type has its own advantages and disadvantages. (Kou 2003, p. 14-15.) The main characteristics of the three current types are presented in Figure 11.

CURRENT TYPE	DCEN	DCEP	AC (BALANCED)
ELECTRODE POLARITY	NEGATIVE	POSITIVE	
ELECTRON AND ION FLOW	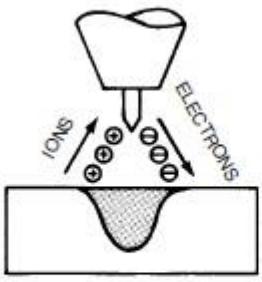	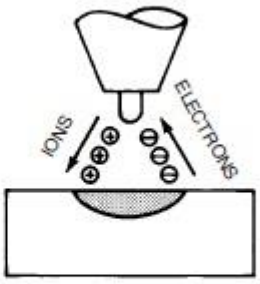	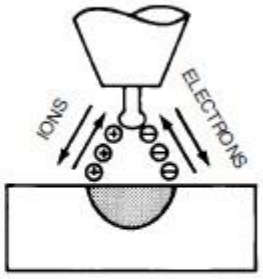
PENETRATION CHARACTERISTICS			
OXIDE CLEANING ACTION	NO	YES	YES—ONCE EVERY HALF CYCLE
HEAT BALANCE IN THE ARC (APPROX.)	70% AT WORK END 30% AT ELECTRODE END	70% AT WORK END 30% AT ELECTRODE END	70% AT WORK END 30% AT ELECTRODE END
PENETRATION	DEEP; NARROW	SHALLOW; WIDE	MEDIUM
ELECTRODE CAPACITY	EXCELLENT e.g., 3.2 mm (1/8 in.) 400 A	POOR e.g., 6.4 mm (1/4 in.) 120 A	GOOD e.g., 3.2 mm (1/8 in.) 225 A

Figure 11. Characteristics of the three different current types used in TIG welding (Salkin et al. 2004, p. 120).

In general TIG welding is at its best when welding thin sheets and high quality is required. It can be used for a large selection of materials such as titanium, aluminum, magnesium, stainless steels and nickel-based superalloys. The process however has lower deposition rates than most other arc welding processes and requires more skill from the welder. Some advantages of TIG welding include (Lienert et al. 2011, p. 345-346, Salkin et al. 2004, p. 105-106):

- High quality welds with low distortion and no spatter.
- Can be used without filler metal.
- The process can be automated with the heat source and filler metal being controlled independently.
- Suitable for almost all metallic materials, also dissimilar ones.
- Welding heat can be controlled accurately.

Main disadvantages of TIG welding are:

- Low deposition rates compared to most arc welding processes.
- Magnetic fields and drafty welding environments can make welding difficult to control.
- Low tolerance for contaminants in both the filler and base metal.
- Brittle tungsten additions in the weld are possible if the electrode is in contact with the weld pool.

5 AUSTENITIC STAINLESS STEELS

Stainless steels are traditionally divided into different categories depending on their microstructure at room temperature, because microstructure is what defines most of the properties of the material. Austenitic grades form the largest group of stainless steels as they possess good formability and weldability and excellent corrosion resistance. (Outokumpu 2013, p. 11-12.) In addition to the chemical composition of the material, the microstructure and properties of the finished product also depend on the manufacturing process.

5.1 Chemical composition and properties

Austenitic stainless steels offer a combination of good mechanical properties and corrosion resistance. They have excellent toughness and ductility even in absolute zero temperature which makes them an optimal choice for cryogenic applications. High-temperature alloys also retain their strength and corrosion resistance at elevated temperatures above 500 °C and possess high creep resistance properties. Due to the diverse range of different alloys and properties, austenitic stainless steels are widely used in such applications as (McGuire 2008, p. 79, Outokumpu 2013, p. 9):

- food and beverage industry
- chemical, oil and gas industry
- transportation
- pulp and paper industry
- kitchen equipment.

Usually the main reason for choosing stainless steels is their corrosion resistance properties, which are caused by a protective chromium oxide layer that forms on the surface of the material. In general, alloys with chromium content of over 10.5 % do not rust in normal environments. Exposure to such elements as seawater or acids can destabilize the protective film resulting in corrosion. To meet the demands of highly corrosive environments, the corrosion resistance properties can be improved by increasing the chromium and molybdenum content of the material. Low-carbon grades of stainless

steel have also been developed in order to increase the welding properties of the material. The lower amount of carbon decreases the occurrence of chromium carbide precipitation which is one of the most common problems in the welding of austenitic stainless steels. (McGuire 2008, p. 71, 84-85.) Chemical compositions of some austenitic stainless steel grades are presented in Table 1.

Table 1. Typical chemical compositions of different kinds of austenitic stainless steel grades (McGuire 2008, p. 72, 86).

Alloy	**C**	**Cr**	**Ni**	**Mo**	**Mn**	**Cu**	**Si**	**N**
304	0.05	18.3	8.1	0.3	1.8	0.3	0.45	0.05
304L	0.02	18.3	8.1	0.3	1.8	0.4	0.45	0.09
316L	0.02	16.4	10.5	2.1	1.8	0.4	0.50	0.03
904L	0.02	19.5	24.0	4.1	1.7	1.3	0.50	0.06
254 SMO	0.02	20.0	18.0	6.1	0.8	0.8	0.40	0.20
654 SMO	0.01	24.0	22.0	7.2	3.0	0.5	-	0.50

5.2 Welding of austenitic stainless steels

The weldability of materials can be evaluated in a number of ways, but different material types require different evaluation methods. For stainless steels one of the most common evaluation methods is the Schaeffler diagram.

The nickel content in austenitic stainless steels maintains a stable austenitic microstructure without the formation of martensite even when the cooling rate is rapid, such as during welding (Kou 2003, p. 432-433). In addition to austenite a certain amount of ferrite will form into the weld metal however. The amount of ferrite that forms depends mainly on the alloying elements which can be divided into austenite formers and ferrite formers. The most common austenite forming elements are nickel, carbon, nitrogen and manganese while ferrite forming elements include chromium, molybdenum, silicon, niobium and aluminum. In order to predict the austenite and ferrite content of the weld in room temperature, a constitution diagram called Schaeffler diagram can be used. The chromium and nickel equivalent of the materials can be calculated using Equations 1 and 2. Then by placing the equivalents into the Schaeffler diagram the microstructure and the typical defects that may develop can be estimated. (Lancaster 1999, p. 318.)

$$Cr_{eq} = (Cr) + (Mo) + 1.5(Si) + 0.5(Nb) \quad (1)$$

$$Ni_{eq} = (Ni) + 30(C) + 0.5(Mn) \quad (2)$$

An illustration of the Schaeffler diagram is presented in Figure 12. Areas where typical welding problems may take place are marked with different colors.

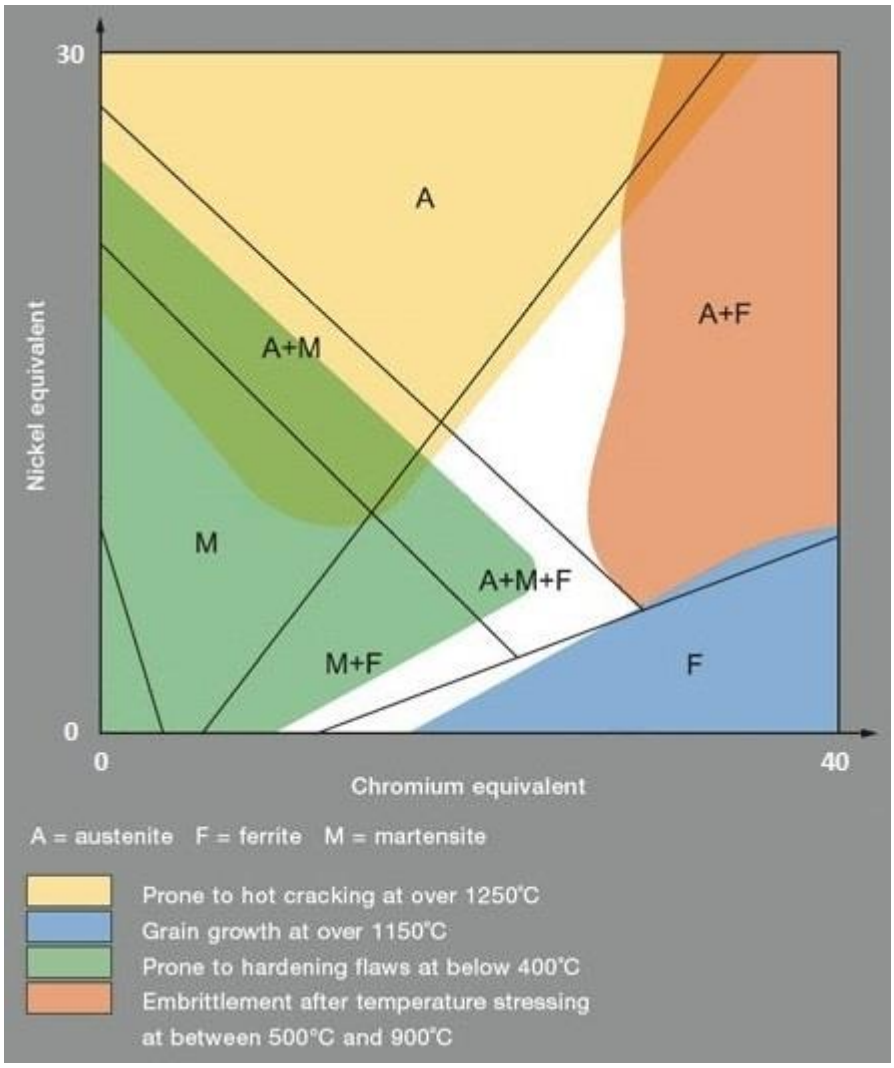

Figure 12. Schaeffler diagram for predicting weld microstructure and typical welding problems in room temperature (Modified from Fronius 2004, p. 19).

The Schaeffler diagram in Figure 12 shows information on what kind of problems may occur in the different microstructural zones as a function of alloying elements. This can also be helpful when choosing a suitable filler metal because in addition to the base

material the filler metal also contributes to the composition of the weld. This way the problematic zones in the diagram can be avoided more easily.

Some of the most common problems when welding austenitic stainless steels include solidification cracking and weld decay (Kou 2003, p. 432). Solidification cracking is affected by the phosphorus and sulfur content of the material and the solidification mode. The vulnerability to cracking is high when solidification is austenitic whereas ferritic-austenitic solidification is the most crack-resistant. This is mainly because the solubility of sulfur and phosphorus is higher in ferrite than it is in austenite. A ferrite content of 3–10 % in the weld metal at room temperature is often desirable in order to control the solidification cracking problem. (Lancaster 1999, p. 319-321.)

In addition to metallurgical factors there are also mechanical factors affecting the occurrence of weld solidification cracking. The relatively high thermal expansion coefficient of austenitic stainless steels can cause solidification shrinkage and stresses during cooling. For example in fillet welds the shape of the weld bead can affect the amount of tension caused by cooling of the weld. A convex weld bead is often desirable in order to reduce tensile stresses in the outer surface of the weld. Also the restraint of the workpiece has an effect on solidification cracking; the greater the degree of restraint, the more likely solidification cracking will occur. (Kou 2003, p. 284, 294.)

Weld decay is a type of intergranular corrosion which is caused by precipitation of chromium carbide at grain boundaries. It can take place in austenitic stainless steels which contain more than 0.05 % carbon. At high temperatures carbon atoms combine with chromium to form chromium carbide at grain boundaries, which depletes the chromium near the grain boundary. Since chromium is the cause of the excellent corrosion resistance in stainless steels the depleted areas are hereby vulnerable to intergranular corrosion. The precipitation of chromium carbide occurs in a temperature range of about 600–850 °C and this is why weld decay appears a short distance away from the fusion boundary where the peak temperature is a bit lower during welding. (Kou 2003, p. 433-437.) The principle of chromium carbide precipitation is presented in Figure 13.

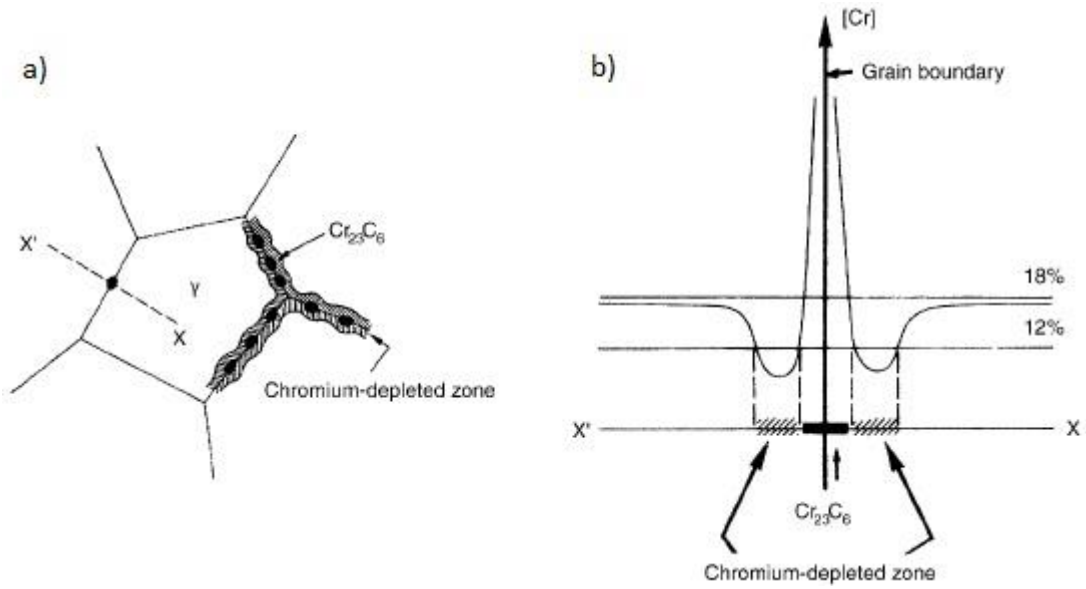

Figure 13. Depletion of chromium near the grain boundaries due to chromium carbide precipitation (McGuire 2008, p. 77).

The carbon content of the material has a direct effect on the occurrence of the weld decay phenomenon. Weld decaying appears more rapidly as the carbon content is increased so it is advisable to use low-carbon steel grades. Also an increase in the heat input widens the region of chromium carbide precipitation and thus the heat input should be limited when possible. A post weld heat treatment in high temperature accompanied with quenching is also a possible remedy for weld decay. (Kou 2003, p. 438-439.)

Heat input is a measure of how much energy is supplied to the weld and it is based on the process parameters that are used during welding. Heat input can be calculated using Equation 3:

$$Q = \eta \times \frac{60 \times U \times I}{1000 \times v} \quad (3)$$

where Q = heat input (kJ/mm)
η = process efficiency factor
U = arc voltage (V)
I = welding current (A)
v = welding speed (mm/min)

The process efficiency factor considers the efficiency of the welding process when determining how much energy actually reaches the workpiece during welding. The process efficiency factor is 0.6 for TIG welding.

It was pointed out before that chromium carbide precipitation can be prevented by using a low heat input during welding. In addition to this the tensile strength and ductility of austenitic stainless steel welds are generally better when a small heat input is used. The size of grains in the heat affected zone (HAZ) is also finer at low heat input. (Kumar & Shahi 2011, p. 3620, 3623.)

5.3 Welding of parts made with selective laser melting

Few publications have been made about the welding of additively manufactured steel parts. Casalino et al. (Casalino et al. 2013, p. 214-215) studied the laser-TIG hybrid welding of SLM stainless steel parts into sheet steel. The test material was 316L stainless steel, similar to the one used in this thesis. It was noticed that the welds exhibited good strength values but elongation was considerably lower than in normal welds of similar steel. In the tensile tests the fracture was brittle and appeared in the SLM side of the joint. This was caused by a sudden increase in the hardness values and could possibly be fixed by heat treating the SLM steel. The stress-strain curves of the weld joints are presented in Figure 14.

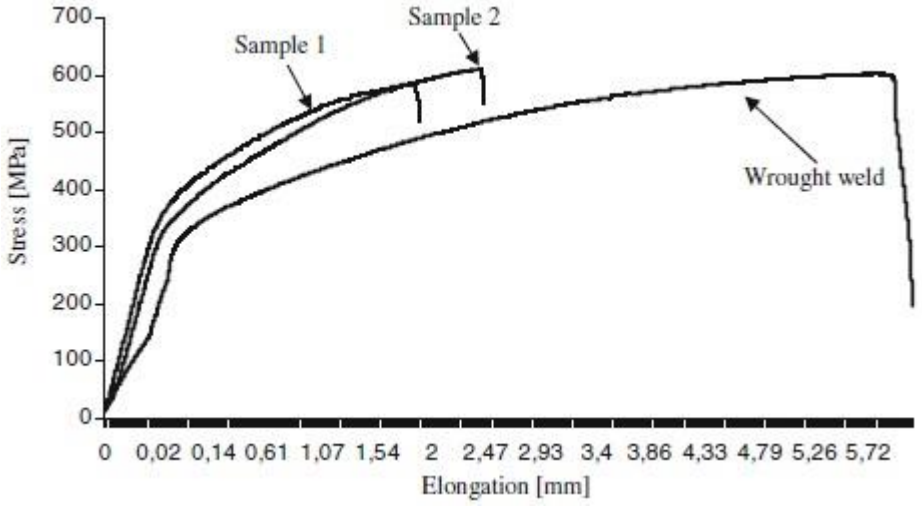

Figure 14. Stress-strain curves of laser-TIG hybrid welded test pieces. Samples 1 and 2 are welds between selective laser melted steel and a similar kind of steel in sheet metal form. (Casalino et al. 2013, p. 214-215.)

In the study of Casalino et al. (Casalino et al. 2013, p. 214-216) the fusion boundary on the SLM steel side of the weld was very sharp and there was no clear heat affected zone. This may be partly due to the nature of the welding process in which heat input is very low. The fusion boundaries on both sides of the weld can be seen in Figure 15. Overall it was concluded that the welding of SLM steel parts is feasible with hybrid laser-TIG welding.

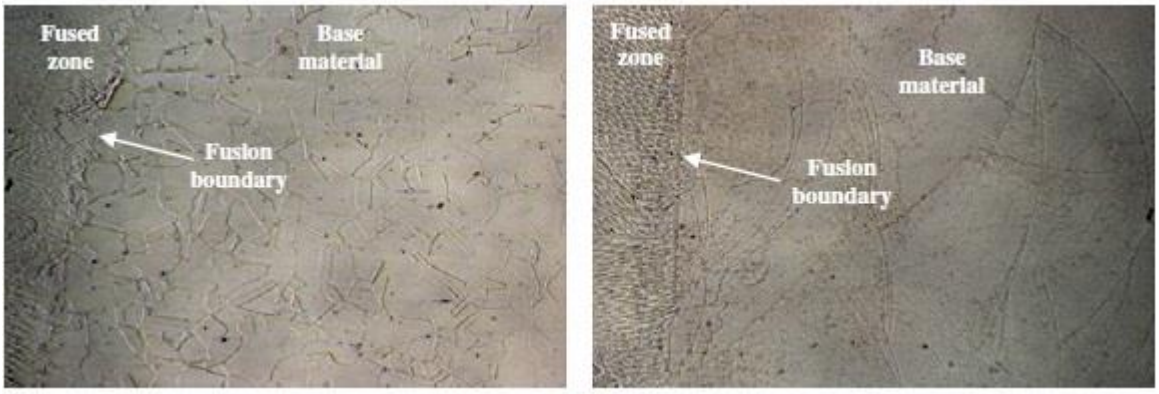

Figure 15. The fusion boundary on the wrought steel side of the weld (left) and on the SLM steel side of the weld (right) achieved with laser-TIG hybrid welding (Casalino et al. 2013, p. 212).

6 DESTRUCTIVE TESTING

Destructive testing means the physical destruction of test pieces in order to evaluate their characteristics. The main objective of destructive testing is to determine the mechanical properties of the material and whether it meets the desired performance requirements. During testing different properties can be studied by subjecting the test pieces to different kinds of stress conditions such as axial tension or compression, bending, torsion and external or internal pressure. (Kuhn & Medlin 2000, p. 49.)

In welded structures loads are typically carried across the weld joints. Destructive testing is also commonly used when inspecting the quality and performance of a weld joint so that the joint fills its mechanical purpose. Mechanical testing of welded joints is often more complicated than the testing of base metal as mechanical properties can vary across the parent metal, heat affected zone and weld metal. Nevertheless the test methods for weld joints are mainly the same than they are for base metal. (Kuhn & Medlin 2000, p. 845-846.)

6.1 Tensile test

Tensile testing is widely used to gain basic information on the strength of the material. A test specimen is subjected to an increasing load and at the same time the elongation of the specimen is observed. This continues until the test specimen ruptures. Based on the load-elongation measurements an engineering stress-strain curve can then be made. From the stress-strain curve the yield strength, ultimate tensile strength and ductility can be evaluated. Figure 16 presents the principle of engineering stress-strain curve. (Kuhn & Medlin 2000, p. 99.)

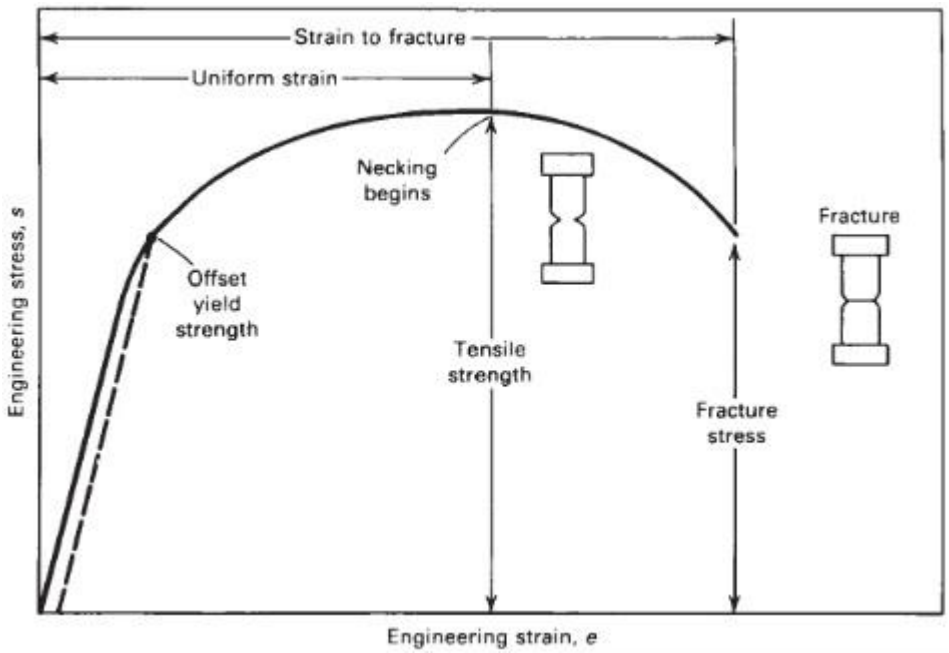

Figure 16. Principle of engineering stress-strain curve (Kuhn & Medlin 2000, p. 99).

At first deformation is elastic and the stress is linearly proportional to strain. When the yield strength of the material is exceeded the deformation becomes plastic which means that the material is now permanently deformed even if the load is reduced to zero. In order to continue the plastic deformation further the required stress increases as the material undergoes strain hardening. Eventually a point is reached where the specimen starts to thin down and the stress required to deform the specimen decreases. The ultimate tensile strength of the material is reached just before the specimen starts to thin down. The stress continues to decrease until the specimen ruptures. (Kuhn & Medlin 2000, p. 99-100.)

The size and shape of test specimen and the test procedure for carrying out transverse tensile tests on welds are specified in the standard SFS-EN ISO 4136:2012 "Destructive tests on welds in metallic materials. Transverse tensile tests". The geometry of tensile test pieces for plates is presented in Figure 17.

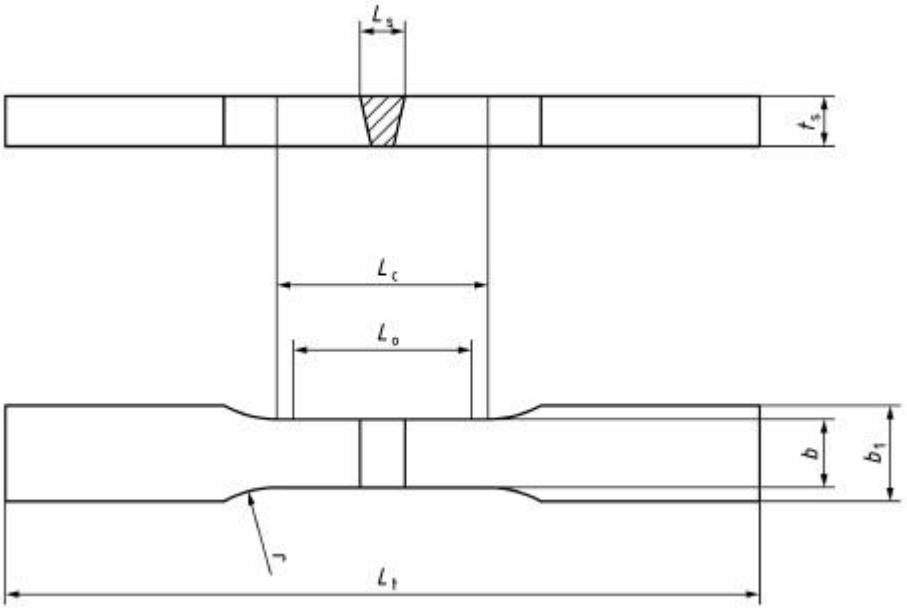

Figure 17. Geometry of tensile test pieces for welded plates (SFS-EN ISO 4136, p. 15).

Yadroitsev et al. (Yadroitsev et al. 2009, p. 1-4) studied the mechanical properties of SLM parts. It was noted that the density of the finished part is an important factor for the properties of SLM parts and that porosity is harmful for strength. Table 2 presents the results of tensile tests carried out in the study. Uneven spreading of powder and the appearance of pores on samples 2 and 3 explain their lower strength properties. Full density was achieved in sample 1 by using different process parameters and scanning strategy than on the other two samples.

Table 2. Results of tensile tests at room temperature for 316L stainless steel SLM test pieces. Lower strength properties of samples 2 and 3 were caused by porosity. (Yadroitsev et al. 2009, p. 5.)

	Ultimate tensile strength (MPa)	**Yield strength (MPa)**	**Elongation (%)**	**Young's modulus (GPa)**
SLM sample 1	555	465	13.5	183
SLM sample 2	383	320	7.0	180
SLM sample 3	369	312	6.0	174

Zhang et al. (Zhang et al. 2013, p. 27-28) also studied the mechanical properties of 316L stainless steel parts made with selective laser melting and had similar results regarding the tensile strength of the parts. It was also noticed that preheating of the building platform had

an increasing effect on the density of the manufactured parts. This also improved the tensile strength and elongation of the parts.

6.2 Bend test

Bend testing is executed in order to determine whether the tested material is ductile. Most other destructive tests give some kind of quantitative result which can be easily compared. The bending ductility test however simply gives either a pass or a fail as a result and the final judgment is done by the test operator. In bend testing the specimen is bended slowly and steadily from the center around a certain radius. After the test the outer surface is observed for cracks as the outside surface is more vulnerable to cracking due to the tension it experiences. The specimen is acceptable if there are no visible cracks on the outside surface. (Kuhn & Medlin 2000, p. 172-174.) There are numerous different kinds of testing devices. One of the most common is an open V-block test device which is presented in Figure 18.

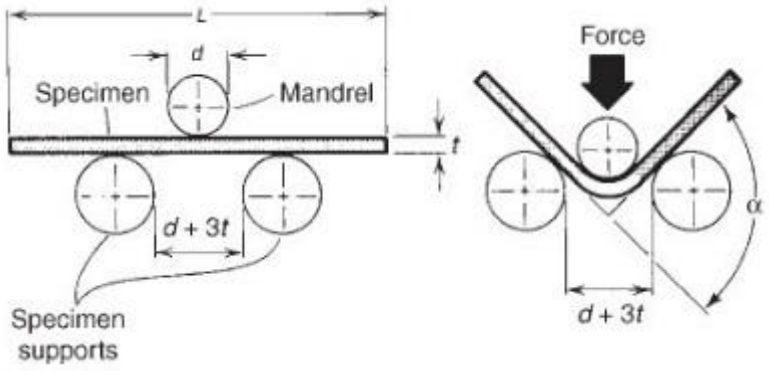

Figure 18. The principle of an open V-block bend test device (Kuhn & Medlin 2000, p. 173).

The test device in Figure 18 consists of a mandrel and two specimen supports. The distance between the supports is adjusted according to material thickness and the specimen is placed on top of the supports. Bending force is then applied to the center of the specimen by pressing the mandrel down until the bend is complete. (Kuhn & Medlin 2000, p. 172-173.)

The dimensions of welded bend test pieces and the details of the testing process are specified in the standard SFS-EN ISO 5173:2010/A1:2011 "Destructive tests on welds in metallic materials. Bend tests". The geometry of a transverse face bend test piece is presented in Figure 19.

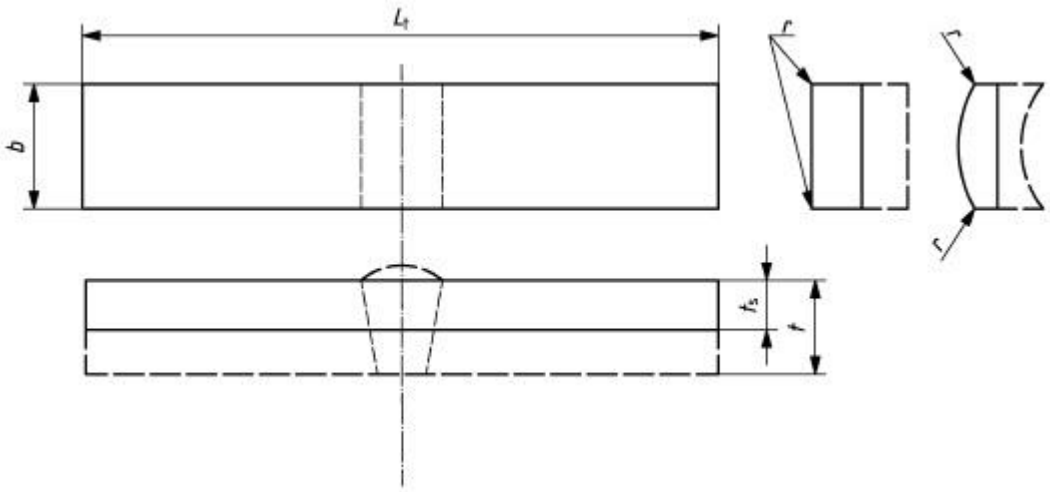

Figure 19. Geometry of face bend test piece for butt welds (SFS-EN ISO 5173, p. 13).

Both the face and root of the weld are usually examined with bend testing in order to make sure there are no imperfections on either surface of the weld. Guidelines for the examination and acceptance of bend test pieces can be found in the standard SFS-EN ISO 15614-1:2004/A2:2012 "Specification and qualification of welding procedures for metallic materials. Welding procedure test. Part 1: Arc and gas welding of steels and arc welding of nickel and nickel alloys".

6.3 Hardness test

Hardness in materials science means the ability of a material to resist permanent deformation caused by a compressive load. Usually hardness testing involves pressing an indenter into the test material's surface. When the geometry of the indenter and the compressive force are known the hardness can be quantified according to one of a variety of scales. There are several different test types such as Brinell, Rockwell and Vickers hardness test, each of which uses a different kind of indenter. (Kuhn & Medlin 2000, p. 197.) The pyramid indenter used in Vickers hardness tests is presented in Figure 20.

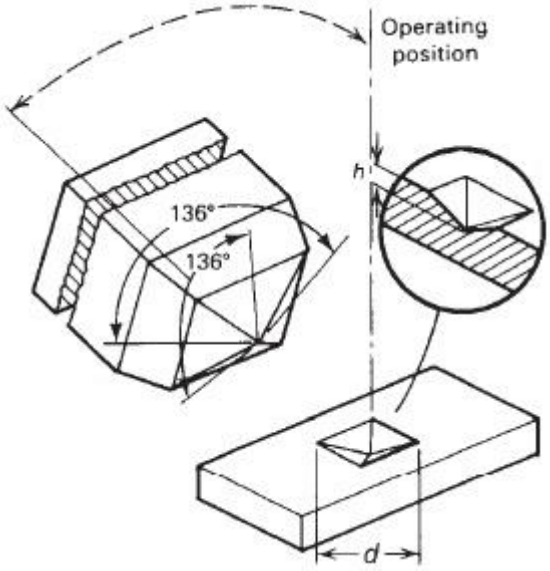

Figure 20. Pyramid indenter used in Vickers hardness testing (Kuhn & Medlin 2000, p. 217).

The area around a weld joint typically has varying microstructures. Hardness testing allows the different regions and microstructures to be compared not only for hardness but also strength, because strength is roughly proportional to hardness. The hardness testing of welds requires a cross-section of the weld joint to be ground, polished and etched. The hardness is then measured from multiple points covering all the different areas of the weld. (Kuhn & Medlin 2000, p. 848.)

The details of hardness testing of arc welded joints are specified in the standard SFS-EN ISO 9015-1:2011 "Destructive tests on welds in metallic materials. Hardness testing. Part 1: Hardness test on arc welded joints". The typical hardness measurement locations in the weld area of a butt weld are presented in Figure 21.

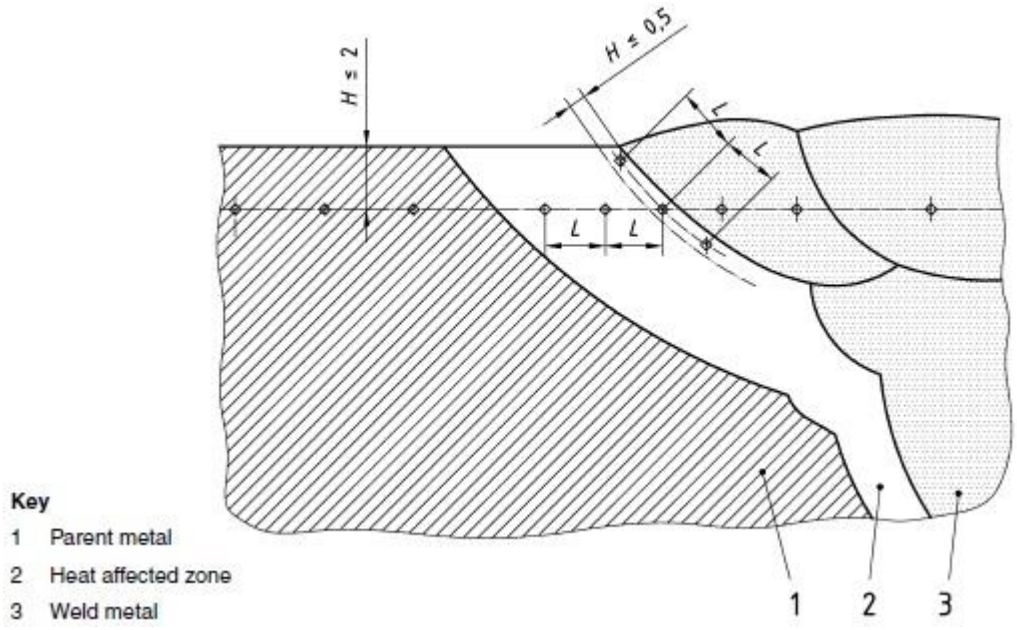

Figure 21. The principle of the location of hardness measurement indentations in butt welds (SFS-EN ISO 9015-1, p. 21).

The spacing and amount of indentations needs to be suitable so that there are multiple measurement points in each zone of the weld area. Additional indentations in the HAZ can be used for materials that harden in the heat affected zone due to welding.

7 EXPERIMENTAL PROCEDURE

The goal of the experimental part was to study the weldability of objects manufactured with selective laser melting and the mechanical properties of the weld joints. The test pieces were welded together with TIG welding using a filler material with chemical composition matching the parent metal. After this the test pieces were machined into tensile and bend test pieces in order to examine their mechanical properties.

7.1 Additive manufacturing equipment

The additive manufacturing equipment that was used in this study was a prototype system made by EOS similar to an EOS EOSINT M-series machine and was located at LUT Laser laboratory. The laser was an IPG YLS-200-SM-CW fiber laser with the maximum output power of 200 W at the wavelength of 1070 nm and the scanner was a Scanlab hurrySCAN 20. The system is presented in Figure 22.

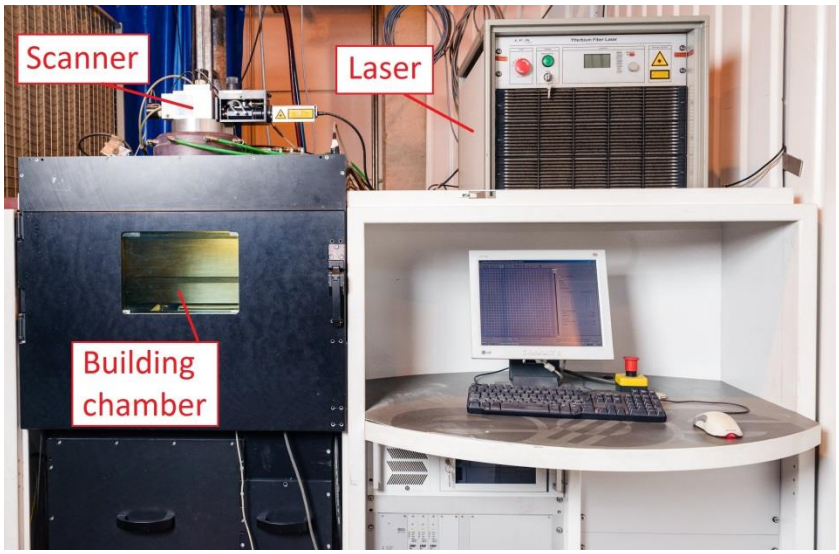

Figure 22. Additive manufacturing equipment used in the study.

The laser beam is transferred from the laser source to the scanner using an optical fiber. The actual building takes place in the building chamber and the process is controlled with a computer. The building chamber where the parts are built consists of a recoater and three

different platforms, each with its own function. The building chamber and its different components are presented in Figure 23.

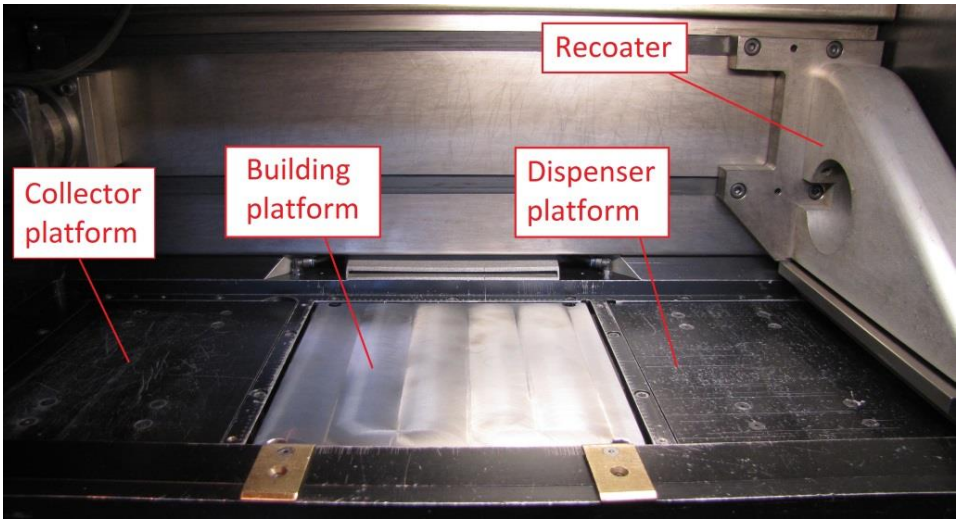

Figure 23. Building chamber of the additive manufacturing system.

First the building platform, which is a milled steel plate, is inserted into the chamber and fastened. Then the building platform needs to be adjusted so that the gap between the platform and the recoater is around 20 μm, which is equal to one layer thickness. This will enable the first layer of powder to be spread evenly on the platform. Next the powder is inserted on the dispenser platform and the chamber is sealed. Before the process is started the building platform is heated to the temperature of 80 °C and the chamber is filled with nitrogen gas in order to avoid the oxidation of the part's surface. The content of nitrogen in the chamber during the process is around 99.8 %. Finally the first layer of powder is spread on the building platform and the actual process can be started. During the building process the powder is spread repeatedly from the dispenser platform to the building platform one layer at a time with the recoater, which moves back and forth in the building chamber to carry out this task. The parts are built on the building platform and the excess powder is collected on the collector platform during recoating.

7.2 Material

The test material for the SLM parts that was used in the study was EOS 316L stainless steel powder. Powder from two different batches was used in the experiments. The chemical composition of the materials is presented in Table 3.

Table 3. The chemical compositions of EOS 316L stainless steel powder (EOS Finland).

Element	**C**	**Cr**	**Ni**	**Mo**	**Mn**	**Cu**	**P**	**S**	**Si**	**N**
Measured value Batch 1 (%)	0.009	17.9	14.2	2.67	1.48	0.01	<0.01	0.007	0.51	0.03
Measured value Batch 2 (%)	<0.01	18.5	14.5	2.5	1.0	<0.05	<0.01	<0.01	0.5	<0.05
Composition Min. (%)		17.00	13.00	2.25						
Composition Max. (%)	0.030	19.00	15.00	3.00	2.00	0.50	0.025	0.010	0.75	0.10

The EOS 316L material is a low-carbon austenitic stainless steel, the chemical composition of which is corresponding to the ASTM F138 (18Cr-14Ni-2.5Mo) stainless steel material. It has excellent corrosion resistance properties and can be used in such fields as automotive and aerospace industry. Because of the building process being layer-wise however, the manufactured parts exhibit some anisotropic behavior. (EOS 2014, p. 1.) This can be seen from Table 4, which shows some mechanical properties of finished parts made out of this material.

Table 4. Mechanical properties of parts made out of EOS 316L stainless steel powder (EOS 2014, p. 4).

Ultimate tensile strength	Horizontal direction (XY)	640 ± 50 MPa
	Vertical direction (Z)	540 ± 55 MPa
Yield strength	Horizontal direction (XY)	530 ± 60 MPa
	Vertical direction (Z)	470 ± 90 MPa
Elongation at break	Horizontal direction (XY)	40 ± 15 %
	Vertical direction (Z)	50 ± 20 %
Hardness		85 HRB

As it can be seen from Table 4, the mechanical properties of the material are somewhat lower in vertical direction than in the horizontal direction. This could be important in some cases and should be kept in mind especially when designing objects that will experience heavy loads. Furthermore, one of the objectives of the thesis is to find out whether the building direction and the resulting anisotropy have any actual effects on the welding properties of the manufactured parts.

A normal 316L (1.4404) stainless steel material, which is the closest standard sheet material available, was decided to be used in the welding experiments as a reference. This way the welding properties of the two materials could be compared more easily. The chemical composition of Outokumpu 316L stainless steel in sheet metal form is presented in Table 5.

Table 5. The typical chemical composition of Outokumpu 316L stainless steel (Outokumpu 2008, p. 1).

Element	**C**	**Cr**	**Ni**	**Mo**	**Mn**	**P**	**S**	**Si**	**N**
Composition Min. (%)		16.00	10.00	2.00					
Composition Typical (%)	0.020	17.2	10.1	2.1					
Composition Max. (%)	0.030	18.00	14.00	3.00	2.00	0.045	0.030	0.75	0.10

As it can be seen from Table 5 the chemical composition of Outokumpu 316L stainless steel sheet is very similar to that of the powder material. The powder material has slightly higher chromium and nickel content and also a smaller tolerance for phosphorus and sulfur, both of which are usually considered impurities in steel materials.

7.3 Test pieces

The parts were designed to be butt welded so that tensile and bend test pieces could be made out of them. In order to achieve this, the parts had to be of certain size and shape while also keeping in mind the limitations of the build volume. A rectangular shape with the dimensions of 100 x 100 x 3 mm was chosen for the test pieces. This would enable one tensile and one bend test piece to be made out of each weld. The digital 3D model of the manufactured pieces is presented in Figure 24.

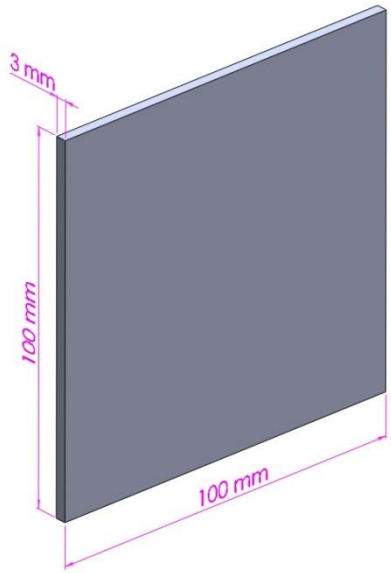

Figure 24. Digital 3D model of the manufactured test pieces.

The test pieces were built on the building platform in a way that minimizes the risk of the recoater colliding with the edge of a part during the manufacturing process. The test pieces were made in two batches. One set of test pieces right after manufacturing is presented in Figure 25.

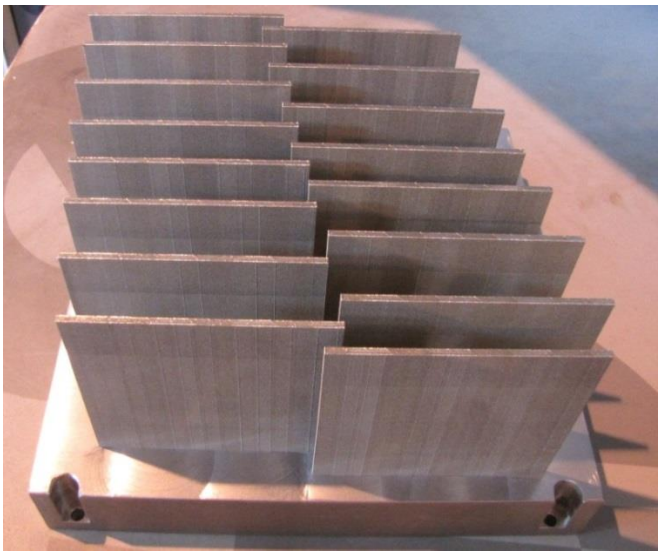

Figure 25. A set of test pieces after manufacturing, still attached to the building platform.

After manufacturing the parts were cut off from the building platform with a MEBAeco 335 G metal bandsaw. The effect of building direction on weld joint properties was studied by making welds in two different orientations as seen in Figure 26.

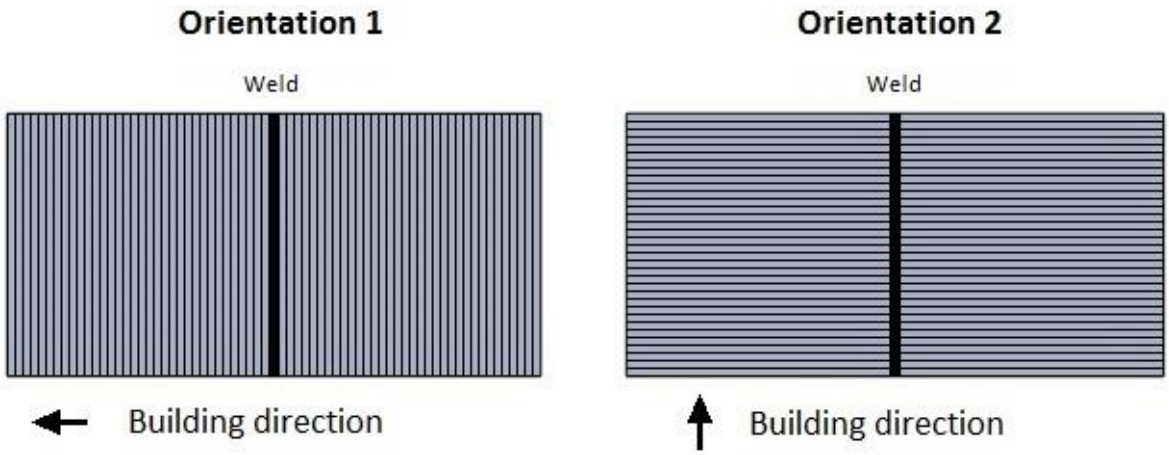

Figure 26. The two different test piece orientations used in the study.

7.4 Welding setup

The welding experiments were conducted at LUT Welding laboratory. The welding machine was a Kemppi MasterTig MLS 3000 ACDC with a Pema welding column and boom for automated welding torch movement. Argon was used as a shielding gas with a gas flow of 10 l/min. A gas lens was attached into the welding torch to improve the shielding gas flow. The welding was done with a single pass from one side and a ceramic weld backing was used. The current type was direct current with electrode negative and the diameter of the tungsten electrode was 2.4 mm. The welding setup is presented in Figure 27.

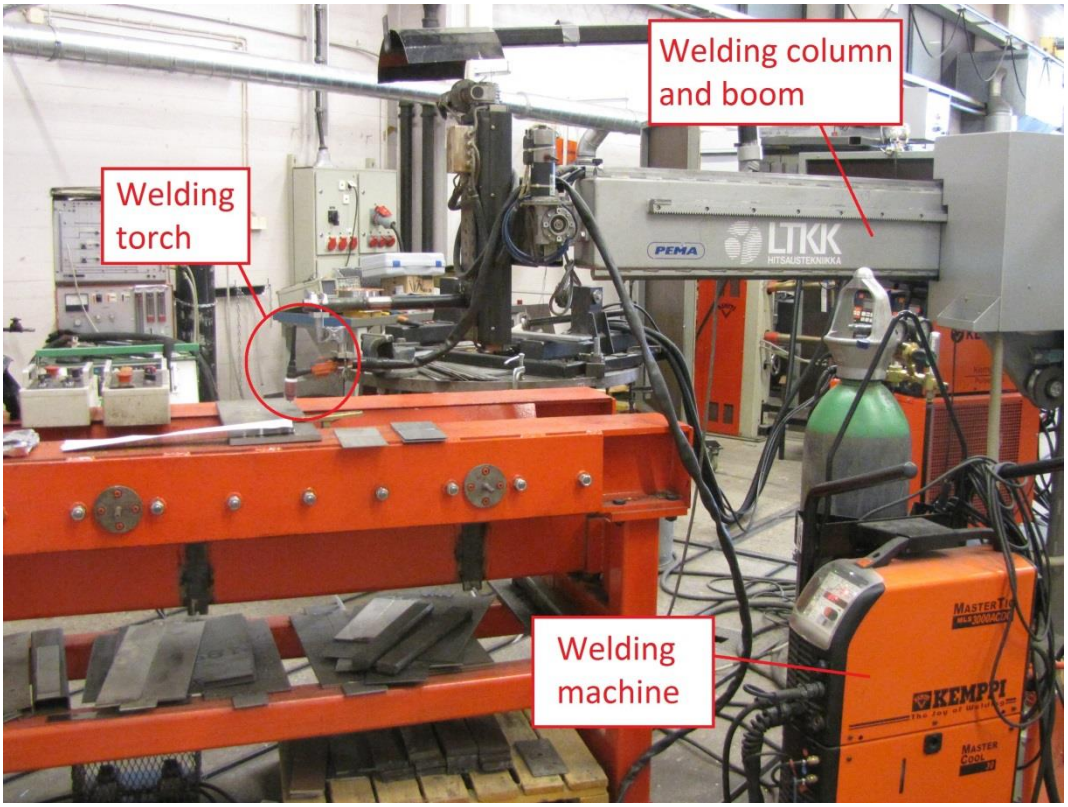

Figure 27. The welding setup at LUT Welding laboratory used in the study.

A bevel angle of 30 ° was machined into each test piece which makes the included angle of each weld 60 °. Additionally a root gap of 1 mm was used between the welded test pieces. Tack welds were used to hold the parts in proper alignment so that the root gap remained the same during the actual welding.

Filler metal feeding was done by hand. A filler metal which had a chemical composition similar to the base material was decided to be used. An Elga Cromatig 316LSi stainless steel wire with a diameter of 2.4 mm was chosen. The chemical composition of the filler metal is presented in Table 6.

Table 6. The chemical composition of Elga Cromatig 316LSi filler metal (Elga 2013, p. 1).

Element	C	Cr	Ni	Mo	Mn	Cu	P	S	Si	N
Composition Min. (%)		18.0	11.0	2.0	1.00				0.65	
Composition Typical (%)	0.015	18.5	12.0	2.7	1.75	0.1	0.015	0.010	0.85	0.06
Composition Max. (%)	0.030	20.0	14.0	3.0	2.50	0.3	0.030	0.020	1.00	

As it can be seen from Table 6 the silicon content of Elga Cromatig 316LSi is slightly higher than that of the parent metal in order to increase the fluidity of the weld metal. Other differences between the parent metal and the filler metal are minor. Based on the chemical compositions of the base materials and the filler metal, the chromium and nickel equivalents were calculated according to Equations 1 and 2 in order to evaluate the weldability of the materials. The chromium and nickel equivalents of the different materials are presented in Table 7.

Table 7. The chromium and nickel equivalents of the materials that were used in the study.

Material	Chromium equivalent	Nickel equivalent
EOS 316L Batch 1	21,3	15,2
EOS 316L Batch 2	21,8	15,3
Outokumpu 316L	19,9	11,2
Elga Cromatig 316LSi	22,5	13,3

Typical composition values were used in the calculations for the Outokumpu and Elga Cromatig materials. By placing the equivalent points into the Schaeffler diagram presented earlier in Figure 12, the diagram indicates that the microstructures of the welds will be austenitic-ferritic and no significant problems due to the alloying elements of the materials should arise.

At the beginning of the welding experiments some preliminary tests were done on sheet metal pieces in order to determine suitable welding parameters that could be used in the actual welding tests. At first the same welding current (180 A) was decided to be used for both the sheet metal and SLM test pieces. During the preliminary welding it was noticed that even though the shape of the test pieces was practically identical, a smaller welding current (150 A) had to be used when welding the SLM test pieces. All of the actual SLM test pieces were then welded with the smaller current. The main welding parameters that were decided to be used in the actual experiments are presented in Table 8.

Table 8. The main welding parameters that were used in the welding experiments and the calculated heat input for both types of test pieces. The heat input is calculated according to Equation 3.

Welding parameter	**Sheet metal test pieces**	**SLM test pieces**
Welding current (A)	180	150
Arc voltage (V)	11	10.5
Welding speed (mm/min)	250	250
Heat input (kJ/mm)	0.285	0.227

All of the process parameters and other welding procedures are presented in the Welding Procedure Specifications (WPS) which can be seen in Appendix I.

7.5 Destructive testing

The dimensions of the tensile test piece are defined by its thickness and by the type of testing machine used. Table 9 presents the dimensions of the tensile test pieces according to SFS-EN ISO 4136 with a material thickness of 3 mm that was used in the study.

Table 9. Dimensions of tensile test pieces used in the study.

Denomination	**Symbol**	**Dimension (mm)**
Thickness of test specimen	t_s	3
Total length of the test specimen	L_t	200
Width of shoulder	b_1	37
Width of the parallel length	b	25
Parallel length	L_c	84

The dimensions of the bend test pieces that were used in the study according to SFS-EN ISO 5173 are presented in Table 10.

Table 10. Dimensions of bend test pieces used in the study.

Denomination	Symbol	Dimension (mm)
Thickness of test specimen	t_s	3
Total length of the test specimen	L_t	200
Width of test specimen	b	12

Considering the width of each test piece it was decided to make one tensile and one bend test piece out of each weld. Also a macrographic section for measuring the hardness in the different parts of the weld area could be made this way. A demonstration of the butt weld test piece assembly is presented in Figure 28.

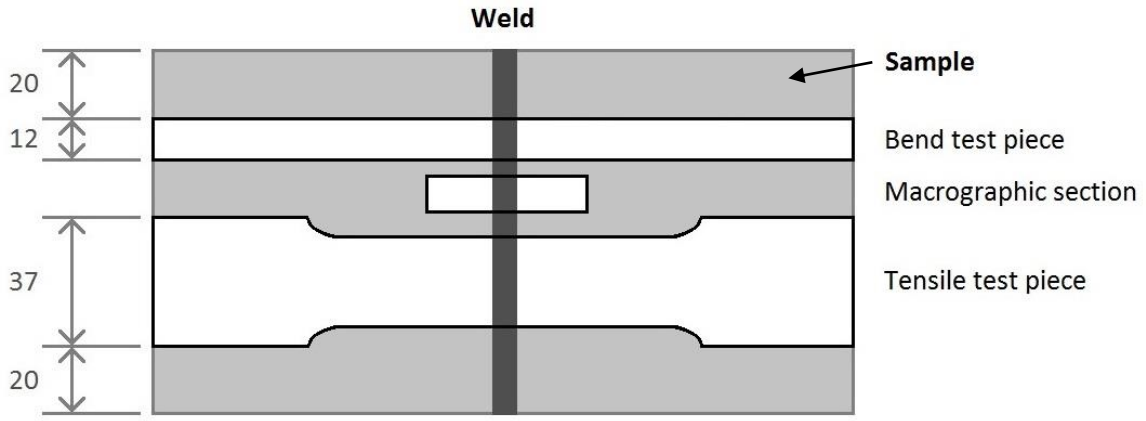

Figure 28. Butt weld test piece assembly used in the study. The gray plate represents the manufactured and/or sheet metal part from which the test pieces were cut off after welding. The weld is situated in the middle.

The bend test pieces were made with a guillotine shear machine and the tensile test pieces were made by milling. Both the tensile and bend tests were conducted with the same machinery at LUT Welding laboratory. The bend test equipment is presented in Figure 29.

Figure 29. Bend test setup used in the study.

The test piece is placed on top of the two parallel support rollers in a way that the weld is located at the center between the rollers. A load is then applied continuously into the center of the test piece with a press tool, which causes bending in the test piece. The diameter of the press tool that was used in the study was 10 mm.

The tensile test setup with a welded test piece placed in the testing machine is presented in Figure 30.

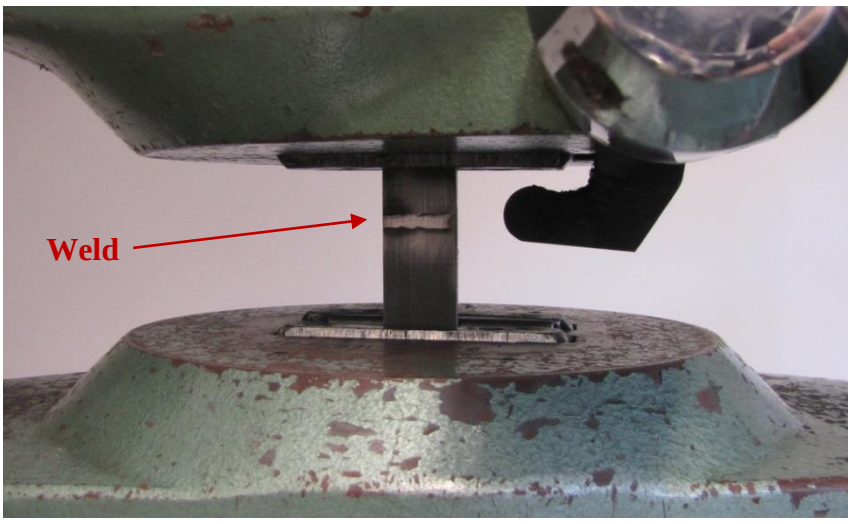

Figure 30. A test piece placed in the tensile test machine.

The test piece is positioned vertically in the testing machine with each end locked in place. The weld is situated in the center area. During the actual testing a tension force is applied into the test piece which causes it to stretch and eventually break. The forces and elongations during testing are measured and transferred directly into a computer. Hardness testing was done with a Struers DuraScan-70 automatic testing device which is presented in Figure 31.

Figure 31. Struers DuraScan-70 automatic hardness testing device used in the study.

The measurement points and other data are inserted into the computer software after which the test device makes the measurements automatically and calculates the hardness values based on the size of the indentations.

7.6 Analysis equipment

A section that was cut from a welded test piece was first polished and then etched with a solution consisting of water and 10 % oxalic acid $(COOH)_2$. An electric current was also used in the etching process. The current was 1.5 A, voltage was 20 V and the etching time was one minute. Micrographs were then taken from the different areas of the weld with an Olympus PME metallurgical microscope system which is presented in Figure 32.

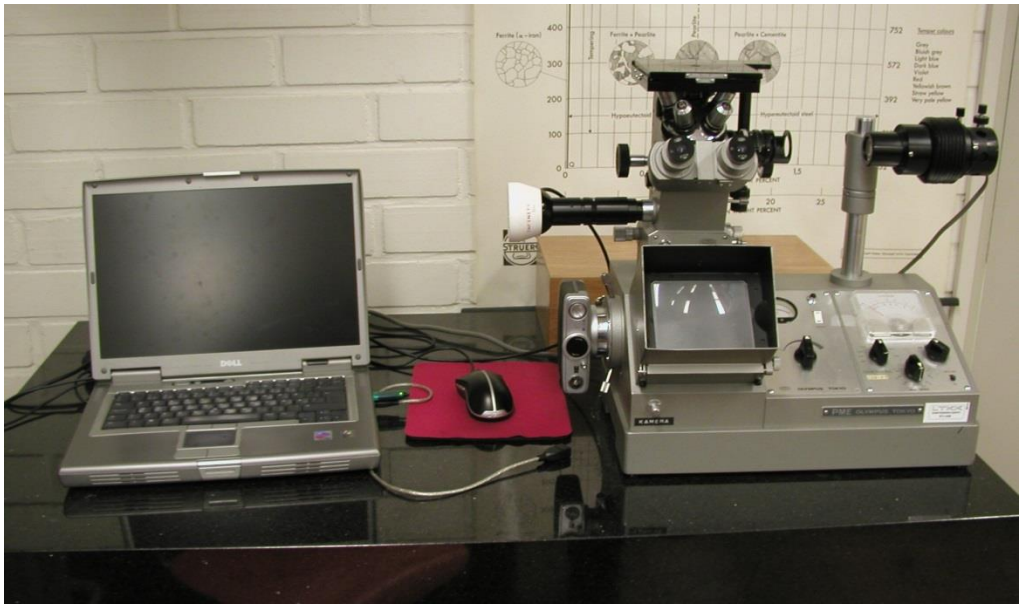

Figure 32. Olympus PME metallurgical microscope equipment used in the study.

The ferrite content of the polished and etched test pieces was measured from multiple points in the weld area with a Feritscope MP3 measurement device. The measurement equipment was based on magnetic induction so measuring was non-destructive. The Feritscope MP3 measurement device is presented in Figure 33.

Figure 33. Feritscope MP3 ferrite content measurement device.

8 RESULTS AND DISCUSSION

The results of the experimental part are presented in this chapter. The chapter is divided into two parts: the results of destructive testing and microstructural analysis of the weld joints. The differences between the welded sheet metal specimens and SLM specimens are also compared in this chapter.

Visual inspection of the welds revealed no imperfections. Figure 34 presents a typical weld surface of one of the welded sheet metal specimens.

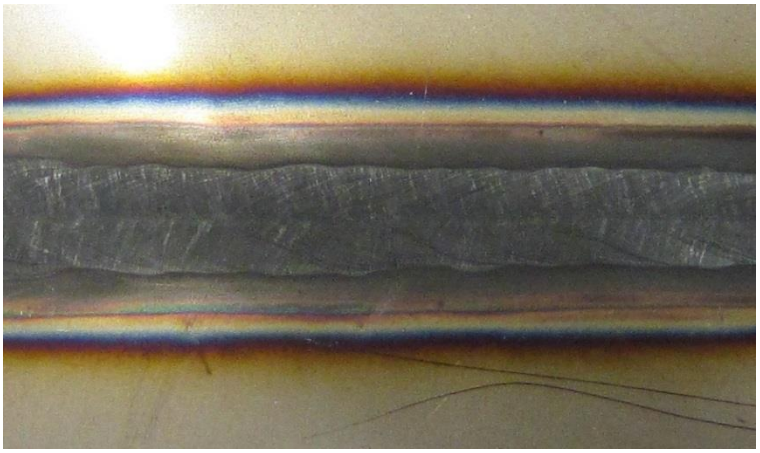

Figure 34. A typical weld surface in one of the sheet metal test pieces.

Some observations on the welding of SLM steel were made before the destructive tests. Like it was pointed out on page 46 a smaller heat input, compared to the one used in sheet metal welding, had to be used when welding the SLM test pieces. Based on the visual evaluation of the welder, the viscosity of the molten pool was initially lower and the welding process was difficult to control with the higher heat input. The reason for this could be due to a number of things including differences in the chemical compositions of the test materials and differences in material properties such as thermal conductivity. The filler metal that was used could also be unsuitable for the SLM test pieces because of its added silicon content, which increases the fluidity of the weld.

By lowering the welding current a clean weld with no apparent defects was achieved and all of the SLM test pieces for the destructive tests were welded with the smaller current. Figure 35 presents the typical weld surface of one of the SLM specimens that was welded using the smaller heat input.

Figure 35. A typical weld surface in one of the SLM test pieces.

8.1 Results of destructive tests

The tensile, bend and hardness tests were carried out as described in the previous chapter. Sheet metal test pieces were also tested in all of the destructive tests to make comparison of the weld joints easier.

8.1.1 Tensile tests

Transverse tensile tests were executed on the milled tensile test pieces in order to examine the yield strength, tensile strength and elongation of the weld joints. The results of all the tensile tests are presented in Table 11. In the SLM specimens O1 means test piece orientation 1 and O2 means test piece orientation 2 (see Figure 26).

Table 11. The results of the tensile tests.

Test piece		Yield strength (MPa)	Ultimate tensile strength (MPa)	Elongation at break (%)
Sheet metal	1	341	576	40
	2	320	561	38
	Average	**331**	**569**	**39**
SLM O1	1	453	518	31
	2	451	518	32
	3	449	520	28
	4	469	539	31
	5	469	543	37
	6	476	560	34
	7	440	523	38
	8	457	526	18
	9	448	520	41
	Average	**457**	**530**	**32**
SLM O2	1	548	643	16
	2	543	631	15
	3	533	624	13
	4	535	624	16
	Average	**540**	**631**	**15**

It can be seen that the yield strength of the SLM specimens in both orientations is considerably higher than that of the sheet metal specimens. The average yield strength of the SLM welds in orientation 1 is 457 MPa whereas for the sheet metal welds it is 331 MPa. Orientation 2 has even higher yield strength with an average of 540 MPa. The average ultimate tensile strength is a little higher in the sheet metal welds compared to the welds in orientation 1. The average ultimate tensile strength is 530 MPa for the welds in orientation 1 and 569 MPa for the sheet metal welds. The highest ultimate tensile strength was observed in orientation 2 with an average of 631 MPa. Elongation at break is highest in the sheet metal welds at 39 %. The orientation of the test pieces affects the elongation greatly, as the elongation at break is over twice as much in orientation 1 than it is in orientation 2.

The strength of the weld joints was about the same as it was for the base material in the study of Yadroitsev et al. (2009) seen on page 33. Also the same observations can be made about the effect of building direction on mechanical properties, as in Table 4. The strength of the material is higher in the horizontal direction than in the vertical direction but

elongation is lower. Elongation at break was higher for the weld joints than it was for the base material in Yadroitsev's study, but lower than the mechanical properties of the material shown in Table 4.

Stress-elongation curves were created based on the data measured with a sensor during the tensile tests. The stress-elongation curves of all the tensile test specimens are presented in Figure 36.

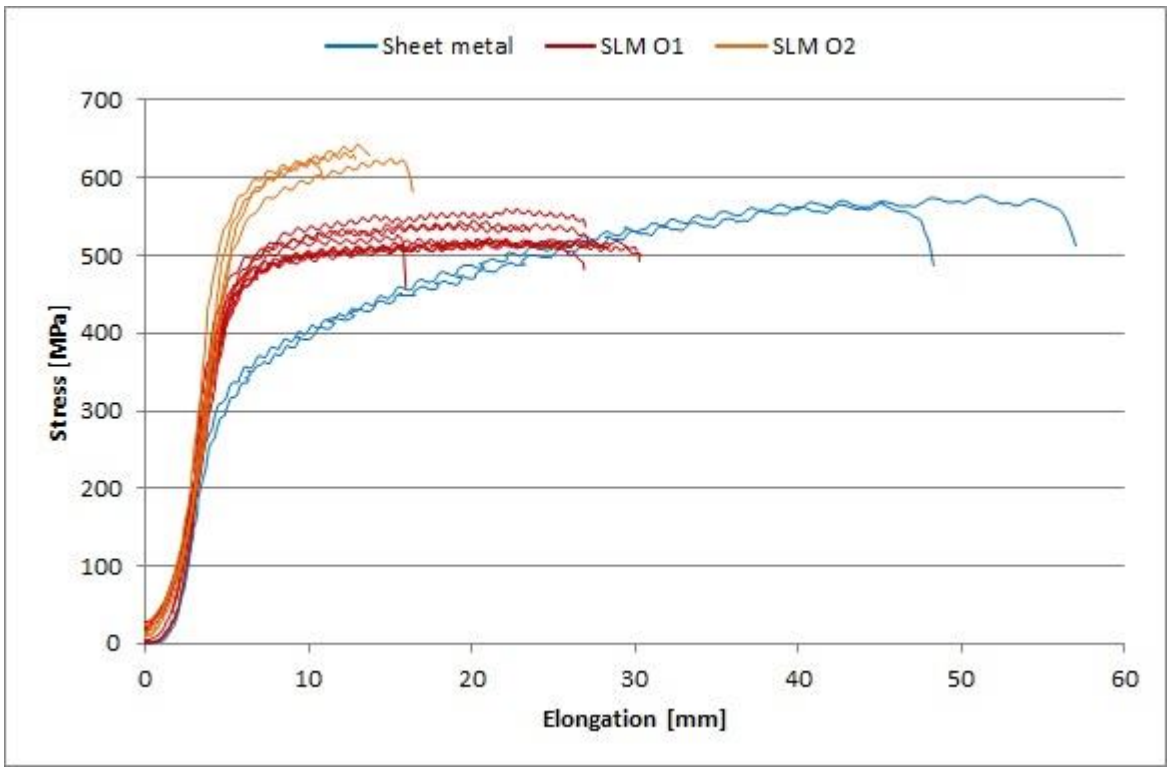

Figure 36. Stress-elongation curves of the tensile test specimens.

Due to the type of sensor that was used in the measurements the elongation values include backlash of the testing equipment and other small inaccuracies. This means that the measured strength values are correct but the resulting stress-elongation curves are not entirely accurate. Nevertheless the general behavior of the different kinds of weld joints can be seen from the curves. Figure 36 shows that the sheet metal test pieces exhibit typical ductile behavior of austenitic stainless steel welds, having a large plastic deformation before fracture. The SLM test pieces in orientation 2 are more brittle since there is only a small amount of plastic deformation before fracture.

Both the sheet metal and SLM specimens ruptured mainly at the heat affected zone near the fusion boundary. Two test pieces in orientation 2 cracked at the center of the weld indicating that the weld metal had lower strength than the parent metal. The fractures of the sheet metal welds were ductile (Figure 37) and the specimens experienced a large amount of plastic deformation and necking before the final fracture.

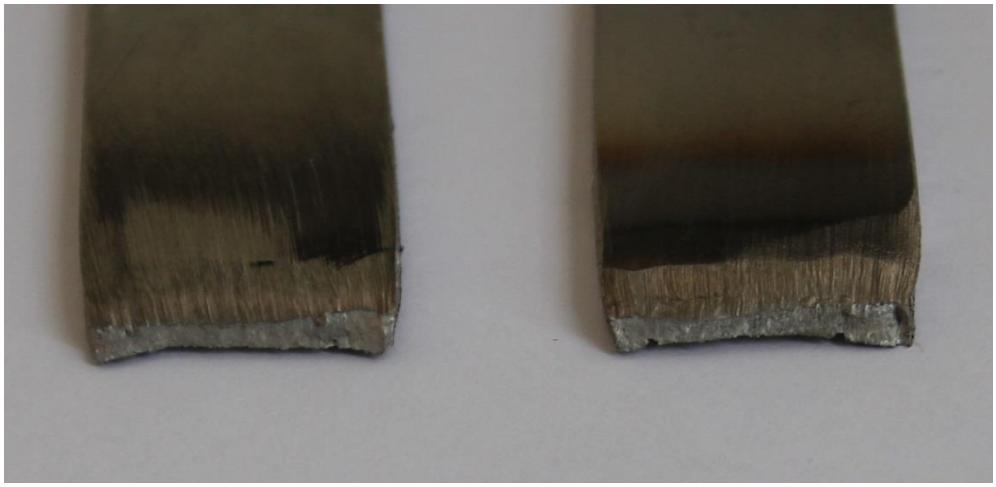

Figure 37. Fracture surfaces of a welded sheet metal test piece.

The fractures of the SLM welds in orientation 1 were not as ductile as the sheet metal welds but not entirely brittle either. The amount of plastic deformation and necking was much smaller. Figure 38 present the fracture surfaces of one of the SLM orientation 1 test specimens.

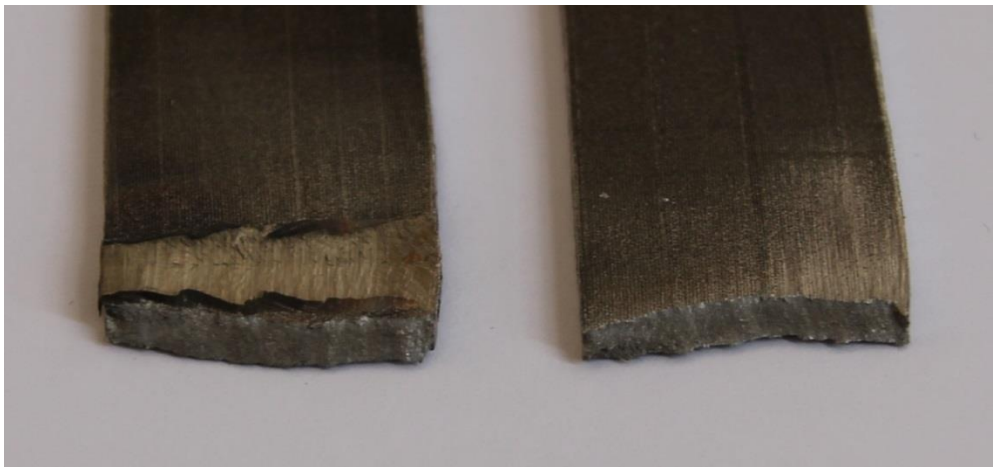

Figure 38. Fracture surfaces of a welded SLM test piece.

A ductile fracture is almost always preferred in materials science. It will take longer for a ductile material to fracture, giving time to notice and repair the problem whereas brittle materials usually fracture suddenly without warning. This may limit the use of brittle materials especially in applications where safety and reliability are the main concerns. The SLM test pieces in orientation 1 demonstrate moderately good ductility but the low elongation of test pieces in orientation 2 means that the weld joints could be too brittle for some applications. It should be kept in mind however that two of the test pieces in orientation 2 fractured near the center of the weld so the strength of the filler metal was too low compared to that of the parent metal.

8.1.2 Bend tests

Both face bend test specimens (FBB) and root bend test specimens (RBB) were tested. Qualification of the test pieces was done according to SFS-EN ISO 15614-1 which allows flaws smaller than 3 millimeters in the specimens. The results of the bend tests are presented in Table 12.

Table 12. The results of the bend tests.

Test piece		Result	Notes
Sheet metal	FBB 1	Pass	
	RBB 1	Pass	
	FBB 2	Pass	
	RBB 2	Pass	
SLM O1	FBB 1	Pass	
	RBB 1	Fail	High weld toe angle
	FBB 2	Pass	
	RBB 2	Fail	High weld toe angle
	FBB 3	Pass	
	RBB 3	Pass	
SLM O2	FBB 1	Pass	Small cracks < 3 mm
	RBB 1	Pass	
	FBB 2	Fail	Cracking near fusion boundary
	RBB 2	Pass	Small cracks < 3 mm

The sheet metal test pieces remained intact during the tests. The relatively low elongation that was discovered in the tensile tests would suggest that the welded SLM specimens might be brittle. A couple of welds had a high weld toe angle on the root side of the weld

which resulted in the failure of the bend test specimens. The geometric discontinuity creates stress concentrations when the angle is too high and the specimens ruptured right at the edge of the weld toe. Therefore the failure of these specimens was due to a defect in the weld joint geometry and not because of the material itself. The other test specimens of orientation 1 remained intact during the test and no defects were found in visual inspection. Test specimens of orientation 2 had low elongation as was noticed in the tensile tests and they were also much more prone to cracking in the bend test. However only one of them actually failed the test because the size of the cracks was within the acceptable level on the other test pieces. Figure 39 presents a root and face bend test specimen after testing.

Figure 39. SLM face and root bend test piece after testing with no visible defects or cracks.

8.1.3 Hardness tests

Hardness tests were executed on one sheet metal and one SLM test piece. Hardness was measured from multiple points at 0.5 mm intervals in the weld area including parent metal, heat affected zone and weld metal. The measurement points of the sheet metal test piece are presented in Figure 40.

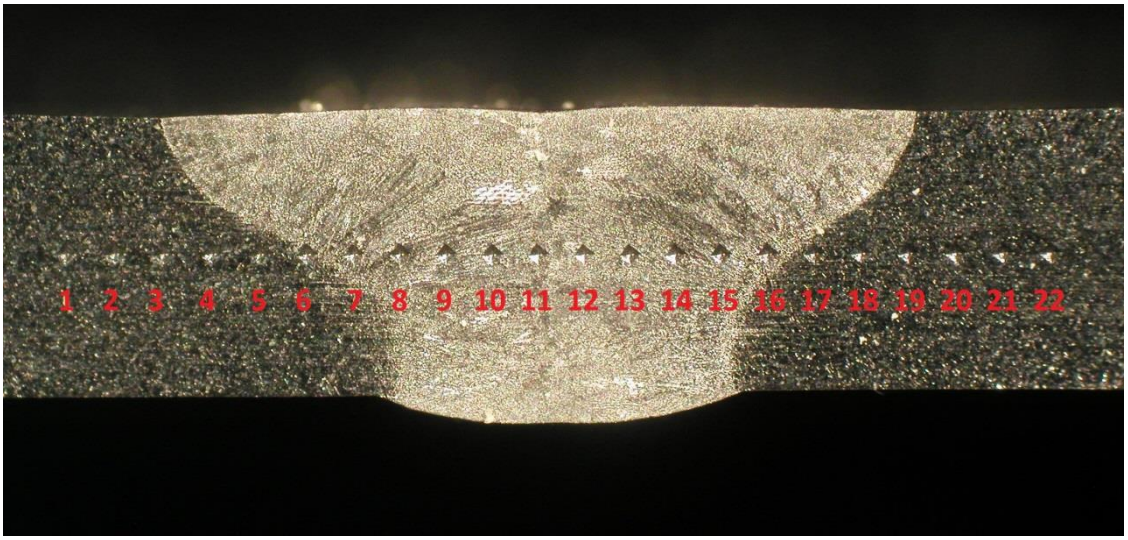

Figure 40. Hardness test measurement points in the weld area of the sheet metal test piece.

Similar tests were executed on a welded SLM specimen. The measurement points of the SLM test piece are presented in Figure 41.

Figure 41. Hardness test measurement points in the weld area of the test piece made with selective laser melting.

The results of the hardness tests are presented in Figure 42.

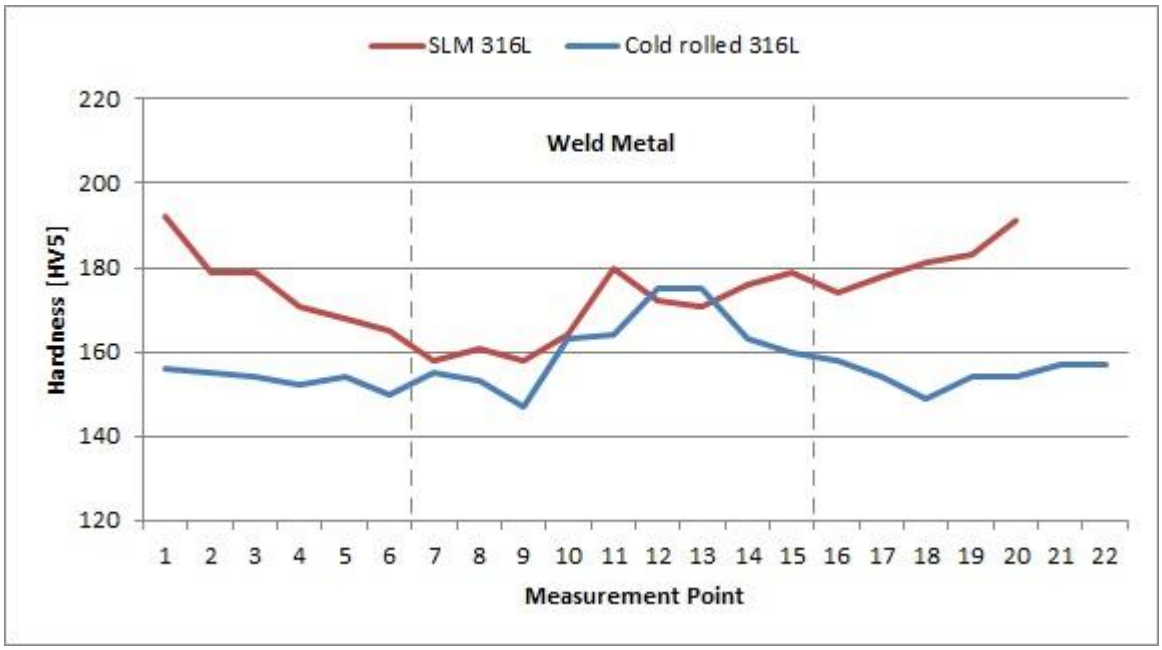

Figure 42. Hardness test results of the weld area of both test pieces. A load of 5 kp was used in the test. The dashed lines represent the fusion boundaries of the welds.

Austenitic stainless steels do not have a tendency for hardening. As it can be noticed from Figure 42 there is not much variation in the hardness values between the parent metal and the weld metal in the case of sheet metal 316L. The weld metal exhibits a little higher hardness values at the center of the weld than in the parent metal. The highest hardness value was 175 HV5 and it was measured near the center of the weld. Also there seems to be practically no change in the hardness values in the fusion boundary or heat affected zone. When it comes to SLM steel the parent metal is actually harder than the weld metal. The highest measured hardness at the weld metal area was 180 HV5 whereas the hardness of the parent metal was around 190 HV5.

8.2 Microstructure analysis

The sheet metal specimens had a typical cold rolled austenitic microstructure and the weld consisted of austenite and ferrite. The fusion boundary of one of the sheet metal welds is presented in Figure 43.

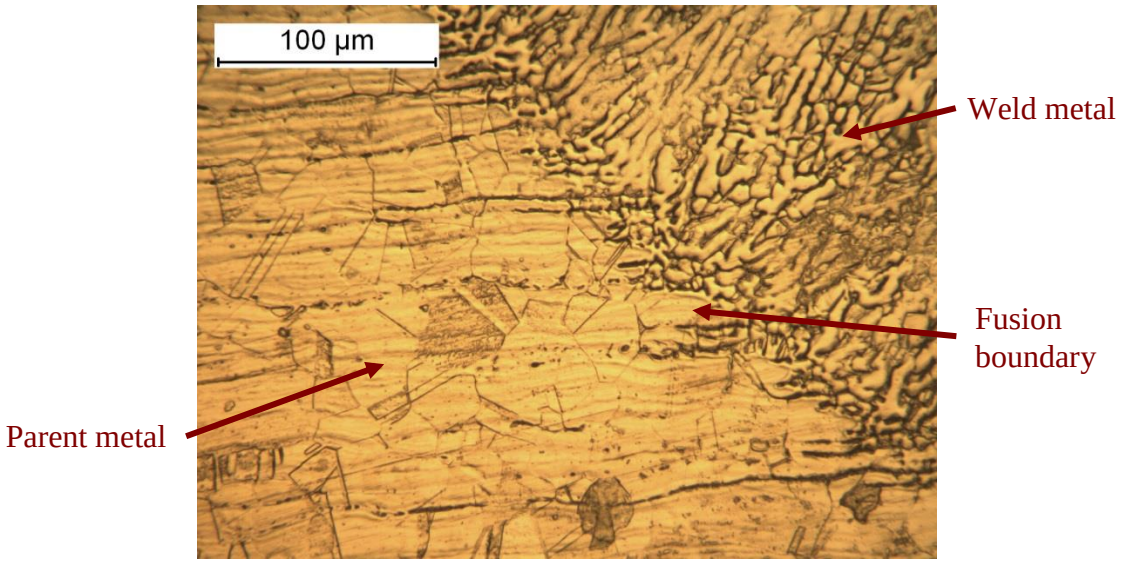

Figure 43. A typical fusion boundary of one of the welded sheet metal test pieces with a 300x magnification.

The fusion boundary in the welded SLM specimen was very sharp as was also noticed from the results of the study by Casalino et al. (2013) on page 30. The fusion boundary of one of the SLM welds is presented in Figure 44.

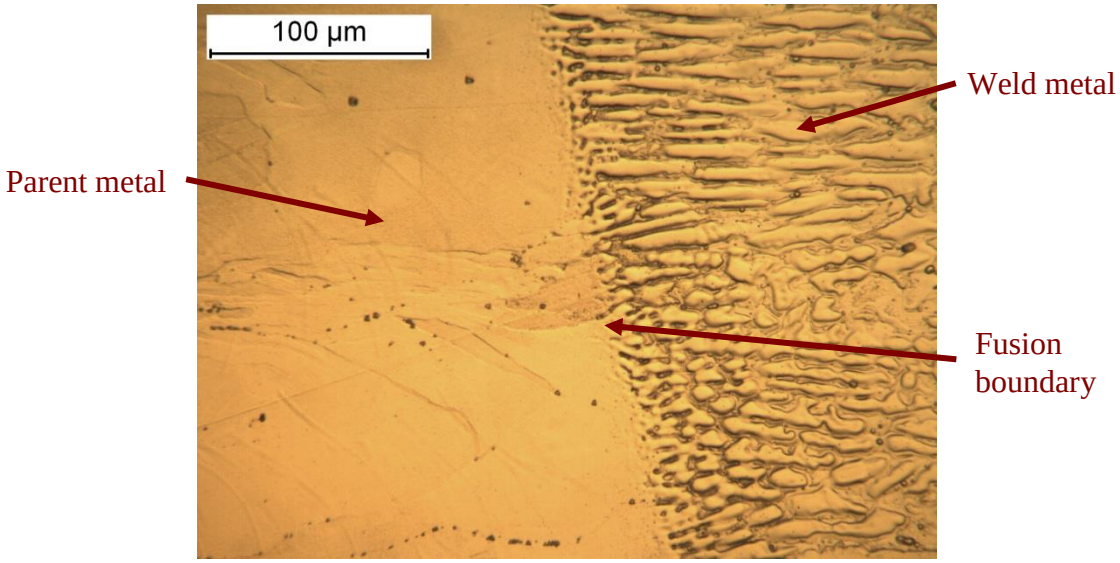

Figure 44. A typical fusion boundary of one of the welded SLM test pieces with a 300x magnification.

Additional micrographs of the parent and weld metal of both specimens are presented in Appendix II. It was stated on page 27 that a ferrite content of 3–10 % in the weld metal helps to prevent solidification cracking. The average ferrite content was measured from one sheet metal and one SLM test piece with a ferrite content measurement device. The results are presented in Table 13.

Table 13. The average ferrite content of the sheet metal and SLM test pieces.

Measurement point	**Sheet metal**		**SLM**	
	Parent metal	**Weld metal**	**Parent metal**	**Weld metal**
1	0.40	5.8	0	6.3
2	0.35	6.5	0	6.9
3	0.28	6.0	0	7.4
4	0.27	6.6	0	7.0
5	0.26	7.0	0	7.7
Average	**0.31**	**6.38**	**0**	**7.06**

It can be noticed from Table 13 that the ferrite content of both the sheet metal and SLM welds was around the same and within the desirable level. It was also notable that there was no ferrite in the parent metal of the SLM test pieces. The sheet metal test piece contained a small amount of ferrite in the parent metal.

9 CONCLUSIONS

The objective of this thesis was to study the weldability of additively manufactured parts and to compare the mechanical properties of the weld joints to those of sheet metal. The material that was studied and used in the tests was a low-carbon austenitic stainless steel EOS 316L. A similar cold rolled 316L stainless steel sheet material was also tested as a reference, to enable easy comparison between the weld joints. Tungsten inert gas welding was used in the welding experiments as it is a suitable process for welding thin stainless steel components.

In the literature part of the study the basic principles of relevant processes such as selective laser melting, tungsten inert gas welding and cold rolling of stainless steels were introduced. It was noticed that the properties of additively manufactured parts vary significantly depending on the building direction. This is due to the fact that the parts are built in layers, which causes anisotropy in the microstructures of the parts. Also the density of the part has a major impact on the mechanical properties of the part, as porosity is harmful for strength.

The experimental part of the study showed that high quality weld joints can be achieved on additively manufactured parts with TIG-welding. Test pieces were decided to be welded in two different orientations to study the effect of building direction on the mechanical properties of the weld joints. Destructive testing of the test pieces was carried out according to standardized tensile, bend and hardness tests and the microstructures of the weld joints were examined with a microscope.

The results of tensile tests exhibited some variation in the properties between the two different orientations, but the yield strength of both orientations was higher than that of the sheet metal welds. However elongation at break was lower in all of the additively manufactured test pieces compared to the sheet metal test pieces. The brittleness of some of the weld joints could be a limiting factor considering the use of welded AM structures in industrial applications, since ductile welds are preferred in order to increase the dependability of the structure. Therefore the building direction and weld joint orientation

should be planned carefully as the different orientations exhibited so much variation in the ductility of the welds.

Most of the test pieces passed the bend test. Some of the specimens which had low elongation appeared to be somewhat brittle and cracks formed near the fusion boundary of the weld during the bend test. Also in this case the test piece orientation had a large effect on how the test pieces behaved during the test. The hardness tests showed that hardening of the heat affected zone was not experienced and that the variation of hardness in the different weld zones was minor. The micrographic examination revealed that the fusion boundary of the additively manufactured test pieces was very sharp and that there was no clear heat affected zone. The ferrite content of the welds was also within the suitable level to prevent solidification cracking.

It can be concluded that TIG-welding is a feasible process for welding additively manufactured parts. There are some key characteristics, such as differences in mechanical properties and the need for different welding parameters that need to be kept in mind when welding components made with additive manufacturing. Also one of the most critical factors that affect the mechanical properties of the weld is the orientation of the test pieces. All in all the welding of AM components opens up new possibilities, since parts that are hard to produce with conventional manufacturing methods can be made with additive manufacturing and then joined to another structure.

10 FURTHER STUDIES

The results of this study showed that TIG welding of additively manufactured stainless steel parts is feasible and that the properties of the weld joints are comparable to those of sheet metal. Many aspects still require further studying however, as there is a large amount of factors that affect the outcome of the weld:

- Other welding processes and materials should be studied to see whether they exhibit similar behavior regarding the tensile and bend tests.
- The surfaces of additively manufactured parts can be rough. The quality and finish of the groove have an impact on welding which means that different kinds of groove preparation methods need to be studied.
- One focus of further studying should be dissimilar joints between additively manufactured and sheet metal parts. This is important because joining an additively manufactured part with an existing structure could be useful for industrial applications.
- The parts could be manufactured in different orientations on the building platform to see how this affects the mechanical properties of the welds.
- Autogenous welding should be tested to see how the weld pool behaves without any filler metal. Different kinds of filler metals should also be tested because in this study two of the welds fractured at the center of the weld, meaning that the weld metal had inferior strength compared to the parent metal.
- Further studying of the metallurgical phenomena that occur during welding and cooling should be done with additional micrographic examination.

REFERENCES

Casalino, G., Campanelli, S. & Ludovico, A. 2013. Laser-arc hybrid welding of wrought to selective laser molten stainless steel. The International Journal of Advanced Manufacturing Technology. Vol. 68, Issue 1, September 2013, p. 209-216.

Chowdhury, S. G., Das, S. & De, P. K. 2005. Cold rolling behavior and textural evolution in AISI 316L austenitic stainless steel. Acta Materialia. Vol. 53, Issue 14, August 2005, p. 3951-3959.

Colás, R., Petrov, R. & Houbaert, Y. 2004. Design of Microstructures and Properties of Steel by Hot and Cold Rolling. Handbook of Metallurgical Process Design. Marcel Dekker, New York. ISBN: 0-8247-4106-4.

Elga. 2013. Cromatig 316LSi Stainless Steel. [Web document] Available at: http://www.google.fi/url?sa=t&rct=j&q=&esrc=s&source=web&cd=3&ved=0CD4QFjAC&url=http%3A%2F%2Fwww.elga.se%2Fmedia%2Fpds%2FEnglish%2FCromatig%25203 16LSi.pdf&ei=KGaVU5vBC8n24QTRqoDgCw&usg=AFQjCNHpp34I69jiVxg_8iU86zHd3Oi_Rw&bvm=bv.68445247,d.bGE [referred: 9.6.2014]

EOS. 2014. Material data sheet – EOS StainlessSteel 316L. [Web document] Available at: http://ip-saas-eos-cms.s3.amazonaws.com/public/77d285f20ed6ae89/32071e4249738be6f1dc5b7bd699164d/EOSStainlessSteel316L.pdf [referred: 8.5.2014]

Fronius. 2004. Weld+vision magazine, No. 12, May 2004. [Web document] Available at: http://www.fronius.com/cps/rde/xbcr/SID-23FF0914-EE3A8B60/fronius_international/40_0006_2136_0104_EN_44757_snapshot.pdf

Gibson, I., Rosen, D. W. & Stucker, B. 2010. Additive Manufacturing Technologies – Rapid Prototyping to Direct Digital Manufacturing. Springer, New York. ISBN: 978-1-4419-1119-3.

Gu, D., Meiners, W., Poprawe, R. & Wissenbach, K. 2012. Laser additive manufacturing of metallic components: materials, processes and mechanisms. International materials reviews. Vol. 57, Issue 3, p. 133-164.

Gu, D. & Shen, Y. 2009. Balling phenomena in direct laser sintering of stainless steel powder: Metallurgical mechanisms and control methods. Materials & Design. Vol. 30, Issue 8, p. 2903-2910.

Hedayati, A., Najafizadeh, A., Kermanpur, A. & Forouzan, F. 2010. The effect of cold rolling regime on microstructure and mechanical properties of AISI 304L stainless steel. Journal of Materials Processing Technology. Vol. 210, Issue 8, p. 1017-1022.

Kamath, C., El-dasher, B., Gallegos, G., King, W. & Sisto, A. 2014. Density of additively manufactured, 316L SS parts using laser powder-bed fusion at powers up to 400 W. The International Journal of Advanced Manufacturing Technology. Vol. 74, Issue 1, September 2014, p. 65-78.

Klar, E. & Samal, P. 2007. Powder Metallurgy Stainless Steels – Processing, Microstructures, and Properties. ASM International. ISBN: 978-0-87170-848-9.

Kou, S. 2003. Welding Metallurgy, 2nd Edition. John Wiley & Sons, New Jersey. ISBN: 0-471-43491-4.

Kruth, J.-P., Badrossamay, M., Yasa, E., Deckers, J., Thijs, L. & Van Humbeeck, J. 2010. Part and material properties in selective laser melting of metals. 16th International Symposium on Electromachining (ISEM), April 2010, Shanghai, China.

Kuhn, H. & Medlin, D. 2000. ASM Handbook, Volume 8 – Mechanical Testing and Evaluation. ASM International. ISBN: 0-87170-389-0.

Kumar, B. R. & Sharma, S. 2013. Recrystallisation characteristics of cold rolled austenitic stainless steel during repeated annealing. Materials Science Forum. Vol. 753, March 2013, p. 157-162.

Kumar, S. & Shahi, A. S. 2011. Effect of heat input on the microstructure and mechanical properties of gas tungsten arc welded AISI 304 stainless steel joints. Materials & Design. Vol. 32, Issue 6, June 2011, p. 3617-3623.

Lancaster, J. F. 1999. Metallurgy of Welding, Sixth Edition. Abington Publishing, Cambridge, England. ISBN: 1-85573-428-1.

Lienert, T., Babu, S., Siewert, T. & Acoff, V. 2011. ASM Handbook, Volume 06A – Welding Fundamentals and Processes. ASM International. ISBN: 978-1-61344-660-7.

McGuire, M. 2008. Stainless Steels for Design Engineers. ASM International. ISBN: 978-0-87170-717-8.

Meiners, W. 2011. Selective Laser Melting – Additive manufacturing for series production of the future? Intermat, February 2011, Luxembourg.

Murr, L., Gaytan, S., Ramirez, D., Martinez, E., Hernandez, J., Amato, K., Shindo, P., Medina, F. & Wicker, R. 2012. Metal fabrication by additive manufacturing using laser and electron beam melting technologies. Journal of Materials Science & Technology. Vol. 28, Issue 1, January 2012, p. 1-14.

Outokumpu. 2008. Type 316/316L stainless steel. [Web document] Available at: http://www.outokumpu.com/SiteCollectionDocuments/Datasheet-316-316l-hpsa-imperial-outokumpu-en-americas.pdf [referred: 11.6.2014]

Outokumpu. 2013. Handbook of Stainless Steel. October 2013, Outokumpu Oyj, Espoo, Finland.

Salkin, J., Beedon, K., Henon, B., Jelonek, K., O'Donnell, D. & Amos, D. 2004. Gas Tungsten Arc Welding. Welding Handbook, 9th Edition – Welding Processes, Part 1. American Welding Society, Edited by Annette O'Brien. ISBN: 978-1-61344-557-0.

SFS-EN ISO 4136. 2012. Destructive tests on welds in metallic materials. Transverse tensile tests. Finnish Standards Association, Helsinki. Approved 10.12.2012.

SFS-EN ISO 5173 + A1. 2011. Destructive tests on welds in metallic materials. Bend tests. Finnish Standards Association, Helsinki. Approved 12.12.2011.

SFS-EN ISO 9015-1. 2011. Destructive tests on welds in metallic materials. Hardness testing. Part 1: Hardness test on arc welded joints. Finnish Standards Association, Helsinki. Approved 23.5.2011.

SSAB. 2011. Steel making process – Sheet steel. [Web document] Available at: http://www.ssab.com/en/Products--Services/About-SSAB/Steel-making-process/Processing/Sheet-steel/ [referred: 29.8.2014]

Yadroitsev, I., Pavlov, M., Bertrand, Ph. & Smurov, I. 2009. Mechanical properties of samples fabricated by selective laser melting. 14èmes Assises Européennes du Prototypage & Fabrication Rapide. June 2009, Paris.

Zhang, B., Dembinski, L. & Coddet, C. 2013. The study of the laser parameters and environment variables effect on mechanical properties of high compact parts elaborated by selective laser melting 316L powder. Materials Science & Engineering: A. Vol. 584, p. 21-31.

APPENDICES

Open your mind. LUT.
Lappeenranta University of Technology

Mechanical Engineering **Welding Procedure Specification**

Parent metal			***Outokumpu 316L (17Cr-12Ni-2Mo)***							
Material thickness			***3 mm***				Groove shape 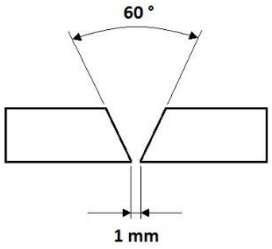		Weld layer sequence 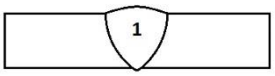	
Pipe outside diameter			-							
Welding process			***141 TIG***							
Welding position			***PA***							
Groove preparation			***Milling***							
Groove cleaning			-							
Workpiece clamping			-							
Tack welding			***141 TIG***							
Weld backing			***Ceramic***				Electrode diameter			***2.4 mm***
	Filler metals and welding gases						Grind angle			-
							Travel angle			***0 °***
	Filler metal classification		***EN ISO 14343 W 19 12 3 LSi*** ***AWS A5.9 ER316LSi***				Work angle			***90 °***
							Distance from workpiece			-
							Temperature			
	Filler metal name		***Elga Cromatig 316LSi*** ***2.4 mm***				Preheating temperature			-
							Interpass temperature			-
							Preheating method			-
	Flux		-				Temperature measurement			-
	Shielding gas		***Ar***				Post weld heat treatment			
	Gas flow		***10 l/min***				Method			-
	Plasma gas		-				Heating rate			-
	Gas flow		-				Temperature			-
	Backing gas		-				Time			-
	Gas flow		-				Cooling rate			-
	Current type		***DC-***				Post processing			-
Notes:							Date and author:			

Bead	Process	Filler metal Ø	Welding current (A)	Arc voltage (V)	Welding speed (mm/min)	Wire feed speed (m/min)	Heat input (kJ/mm)	Oscillation frequency (Hz)	Amplitude (mm)	Notes
1	***141***	***2.4***	***180***	***11***	***250***	***-***	***0.285***	***-***	***-***	***-***

Client:	Approved:

Open your mind. LUT.
Lappeenranta University of Technology

Mechanical Engineering **Welding Procedure Specification**

Parent metal	***EOS 316L (18Cr-14Ni-2.5Mo)***									
Material thickness	***3 mm***						Groove shape		Weld layer sequence	
Pipe outside diameter	-						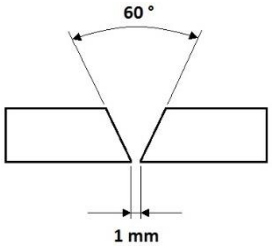		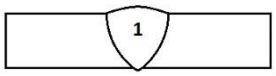	
Welding process	***141 TIG***									
Welding position	***PA***									
Groove preparation	***Milling***									
Groove cleaning	-									
Workpiece clamping	-									
Tack welding	***141 TIG***									
Weld backing	***Ceramic***						Electrode diameter		***2.4 mm***	
	Filler metals and welding gases						Grind angle		-	
							Travel angle		***0 °***	
	Filler metal classification	***EN ISO 14343 W 19 12 3 LSi*** ***AWS A5.9 ER316LSi***					Work angle		***90 °***	
							Distance from workpiece		-	
							Temperature			
	Filler metal name	***Elga Cromatig 316LSi*** ***2.4 mm***					Preheating temperature		-	
							Interpass temperature		-	
							Preheating method		-	
	Flux	-					Temperature measurement		-	
	Shielding gas	***Ar***					Post weld heat treatment			
	Gas flow	***10 l/min***					Method		-	
	Plasma gas	-					Heating rate		-	
	Gas flow	-					Temperature		-	
	Backing gas	-					Time		-	
	Gas flow	-					Cooling rate		-	
	Current type	***DC-***					Post processing		-	
Notes:							Date and author:			

Bead	Process	Filler metal Ø	Welding current (A)	Arc voltage (V)	Welding speed (mm/min)	Wire feed speed (m/min)	Heat input (kJ/mm)	Oscillation frequency (Hz)	Amplitude (mm)	Notes
1	***141***	***2.4***	***150***	***10.5***	***250***	-	***0.227***	-	-	-

Client:	Approved:

APPENDIX II MICROGRAPHS OF WELDED SPECIMENS

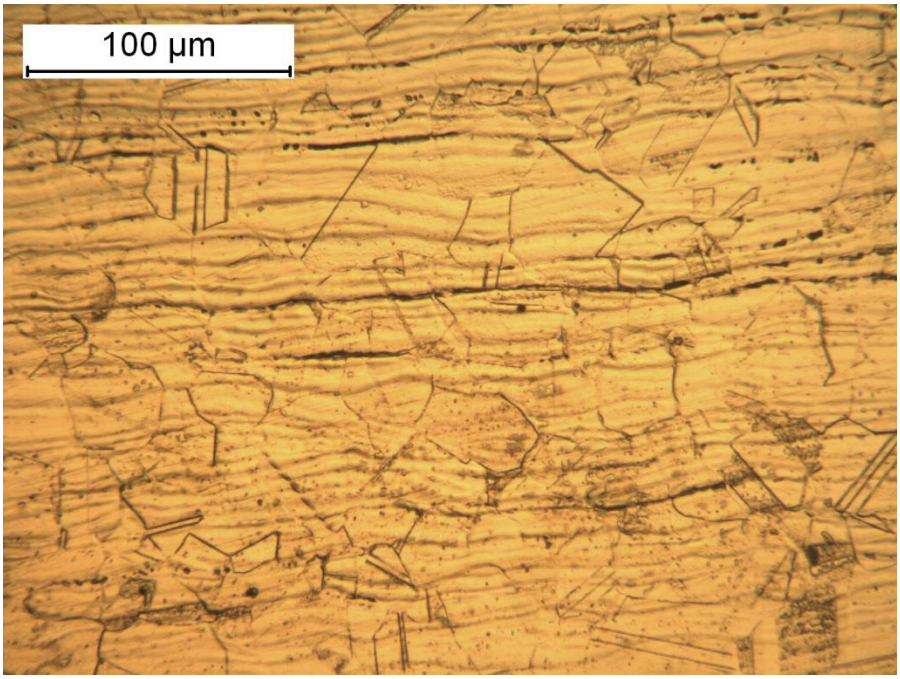

Figure 1. Parent metal of one of the welded sheet metal specimens.

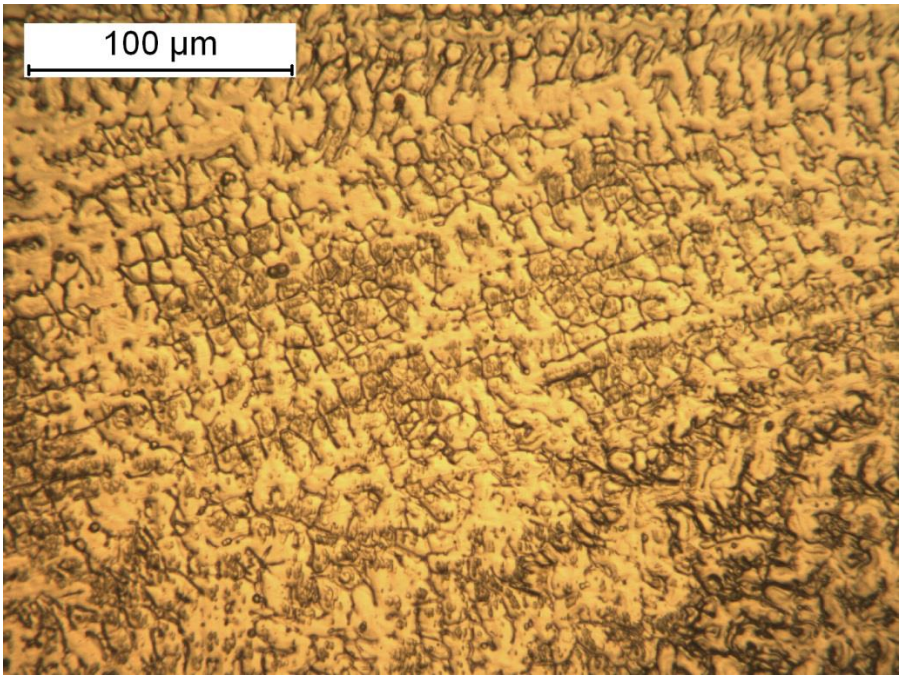

Figure 2. Weld metal of one of the welded sheet metal specimens.

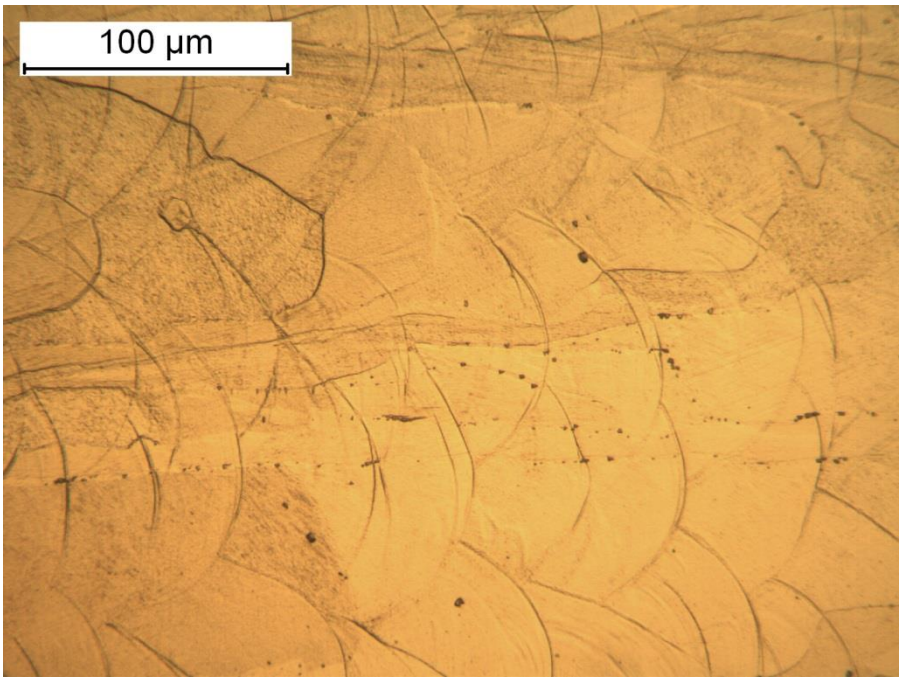

Figure 3. Parent metal of one of the welded SLM specimens.

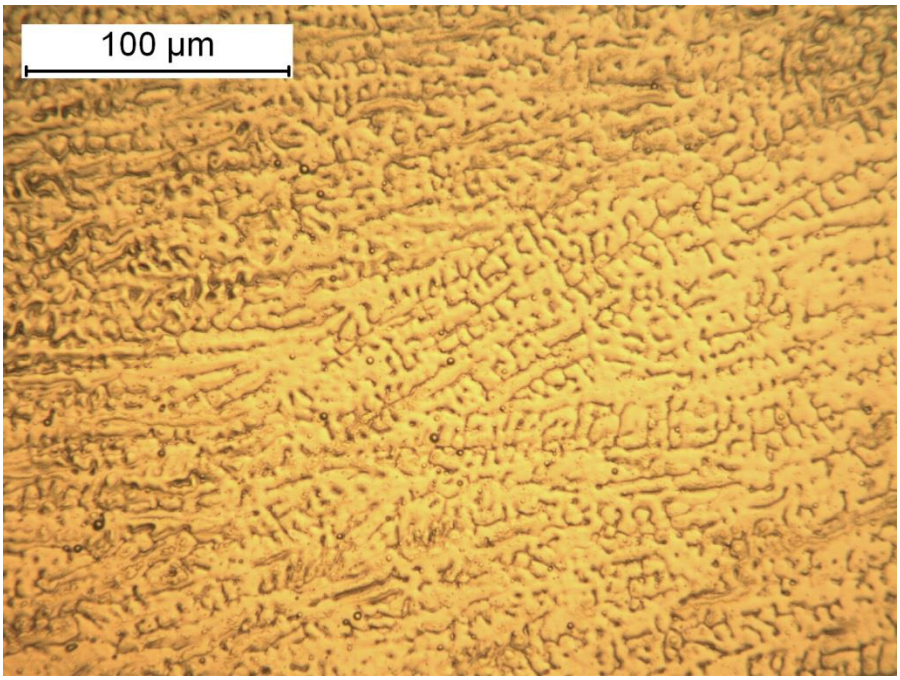

Figure 4. Weld metal of one of the welded SLM specimens.